

For Reference

NOT TO BE TAKEN FROM THIS ROOM

For Reference

NOT TO BE TAKEN FROM THIS ROOM

Ex LIBRIS
UNIVERSITATIS
ALBERTAENSIS



THE UNIVERSITY OF ALBERTA

LAMINAR FREE CONVECTION FROM A
DOWNWARD-PROJECTING FIN

by

JOHN C. GUNN, B.Sc. (Alberta)

A THESIS

SUBMITTED TO THE FACULTY OF GRADUATE STUDIES
IN PARTIAL FULFILMENT OF THE REQUIREMENTS FOR THE DEGREE
OF MASTER OF SCIENCE

DEPARTMENT OF MECHANICAL ENGINEERING

EDMONTON, ALBERTA

April 1967

UNIVERSITY OF ALBERTA

FACULTY OF GRADUATE STUDIES

The undersigned certify that they have read,
and recommend to the Faculty of Graduate Studies for
acceptance, a thesis entitled, "LAMINAR FREE CONVECTION
FROM A DOWNWARD-PROJECTING FIN" submitted by JOHN C. GUNN
in partial fulfilment of the requirements for the degree
of Master of Science.

ABSTRACT

A theoretical and experimental investigation is presented for conduction through and free convection from a tapered, downward-projecting fin immersed in an isothermal, quiescent fluid. The problem is solved by assuming quasi-one-dimensional heat conduction in the fin and matching the solution to that of the convection system, which is treated as a boundary layer problem.

The theoretical analysis undertaken for an infinite Prandtl number reveals a solution which takes the form of a power law temperature distribution along the fin. It is shown that this power (n) is independent of the precise form of the fin profile and is dependent only on a single non-dimensional group χ . The effect of n on heat transfer, skin friction, fin effectiveness and the corresponding boundary layer profiles is discussed. In comparing these results to those from previous work for the unit Prandtl number case, it is demonstrated that the independent effect of Prandtl number is very small for the range $1 \leq \sigma \leq \infty$.

Theoretical predictions were very well verified by the experimental results which consist of temperature profiles and the $n - \chi$ relation for different fin geometries and surrounding fluids.

ACKNOWLEDGEMENTS

The author wishes to thank the following for their contributions:

- Dr. G.S.H. Lock for suggesting an interesting topic and for his supervision of the thesis.
- the members of the Mechanical Engineering Shop, particularly Mr. Bill Kell who built the apparatus and Mr. Ray Marak for his aid in the instrumentation.
- Miss Lynne Fiveland for her patience in typing the thesis.
- the National Research Council for financial support under grant no. A-1672.
- my wife, Diane, for her patience and understanding during the writing of the thesis.

TABLE OF CONTENTS

	<u>PAGE</u>
CHAPTER I <u>INTRODUCTION</u>	1
CHAPTER II <u>THEORETICAL ANALYSIS</u>	5
2.1 BOUNDARY LAYER PROBLEM	5
2.1-1 FORMULATION OF PROBLEM	5
2.1-2 SIMILARITY SOLUTIONS	7
2.1-3 GOVERNING EQUATIONS	9
2.2 SOLUTIONS TO THE BOUNDARY LAYER EQUATIONS..	10
2.2-1 MEKSYN'S METHOD	11
2.2-2 SOLUTION FOR EIGENVALUES	16
2.2-3 VELOCITY AND TEMPERATURE PROFILES...	19
2.3 MATCHING CONDUCTION PROBLEM	19
2.3-1 SOLUTION OF CONDUCTION EQUATION	21
2.3-2 FIN EFFECTIVENESS	22
CHAPTER III <u>EXPERIMENTAL WORK</u>	26
3.1 DESIGN OF APPARATUS	26
3.2 INSTRUMENTATION	30
3.3 EXPERIMENTAL METHOD	31
3.3-1 TESTING PROGRAM	32
3.3-2 PRELIMINARY TESTS	33
3.3-3 TEST PROCEDURE	34
CHAPTER IV <u>DISCUSSION OF RESULTS</u>	36
4.1 HEAT TRANSFER AND SKIN FRICTION	36
4.2 TEMPERATURE INDEX	37

	<u>PAGE</u>
4.3. VELOCITY AND TEMPERATURE PROFILES	42
4.4. FIN EFFECTIVENESS	47
4.5. BOUNDARY LAYER SHAPES	49
CHAPTER V <u>CONCLUSIONS AND RECOMMENDATIONS</u>	53
5.1. CONCLUSIONS	53
5.2. RECOMMENDATIONS	55
<u>REFERENCES</u>	57
APPENDIX A FORTTRAN IV PROGRAM FOR EIGENVALUE SOLUTION	59
APPENDIX B FORTTRAN IV PROGRAM FOR VELOCITY AND TEMPERATURE PROFILES	67
APPENDIX C DATA REDUCTION	70
APPENDIX D ALTERNATIVE SOLUTION	72

LIST OF ILLUSTRATIONS

<u>FIGURE</u>	<u>PAGE</u>
1.1 TAPERED, DOWNWARD-PROJECTING FIN	3
2.1 HEAT TRANSFER AND SKIN FRICTION RESULTS.....	18
2.2 VELOCITY AND TEMPERATURE PROFILES	20
2.3 DETERMINATION OF TEMPERATURE INDEX	23
2.4 FIN EFFECTIVENESS	25
3.1 DIAGRAMMATIC VIEW OF APPARATUS	27
3.2 PICTORIAL VIEW OF APPARATUS	28
4.1 COMPARISON OF $n - \chi$ RELATION	40
4.2 COMPARISON OF TEMPERATURE PROFILE (GLYCERINE)	44
4.3 COMPARISON OF TEMPERATURE PROFILE (WATER)	45
4.4 SCHLIEREN PHOTOGRAPH ($n < 0.2$)	51
4.5 SCHLIEREN PHOTOGRAPH ($n > 1$)	52
TABLE I SUMMARY OF TEST RESULTS	39

NOMENCLATURE

x	vertical distance above fin tip
y	lateral distance from fin surface
w	fin length
δ	fin half width
λ	fin half angle
m	fin shape index
β	thermal expansion coefficient
κ	thermal diffusivity
ν	momentum diffusivity
ρ	fluid density
c_p	specific heat at constant pressure
σ	Prandtl number
g	gravitational acceleration
P	pressure
P_s	hydrostatic pressure
P_d	pressure due to thermal or viscous effects
\tilde{V}, u, v	velocity
T, θ, ϕ, Φ	temperature
ψ, f, F	stream function
η, ξ	similarity variable
n	temperature index
\mathbb{H}	dissipation function
'	denotes differentiation with respect to ξ

H, τ, Q, R	functions defined in text
a, b, b', c, A, d, g	coefficients in power series
α, γ	eigenvalues
Γ	gamma function
k	thermal conductivity
h	heat transfer coefficient
χ	non-dimensional group defined in text
ϵ	fin effectiveness
t	time
\tilde{G}	body force per unit mass

SUBSCRIPTS

R	root
o	surface
s	solid fin
f	fluid surrounding fin
σ	dependent on σ
n	dependent on n

CHAPTER I

INTRODUCTION

It is well known that extending the basic heat transfer surface by means of fins considerably increases the rate of heat transfer from a surface immersed in an isothermal, quiescent fluid. The quantity most frequently used in evaluating the performance of fins is fin effectiveness. In the past [1]*, fin effectiveness has been based on the solution of the conduction problem with the convective boundary condition given by an empirical, constant value of heat transfer coefficient.

Generally the surface heat transfer coefficient is not constant but is some function of distance along the fin surface and therefore particular attention must be given to its form. For a vertical fin as considered in the following analysis, the problem may be solved by treating it as a quasi-one-dimensional conduction problem with the convective boundary condition obtained from the solution of the boundary layer problem. First this entails solving the problem of laminar free convection from a vertical, nonisothermal surface. Secondly, the surface temperature and heat flux in the corresponding conduction

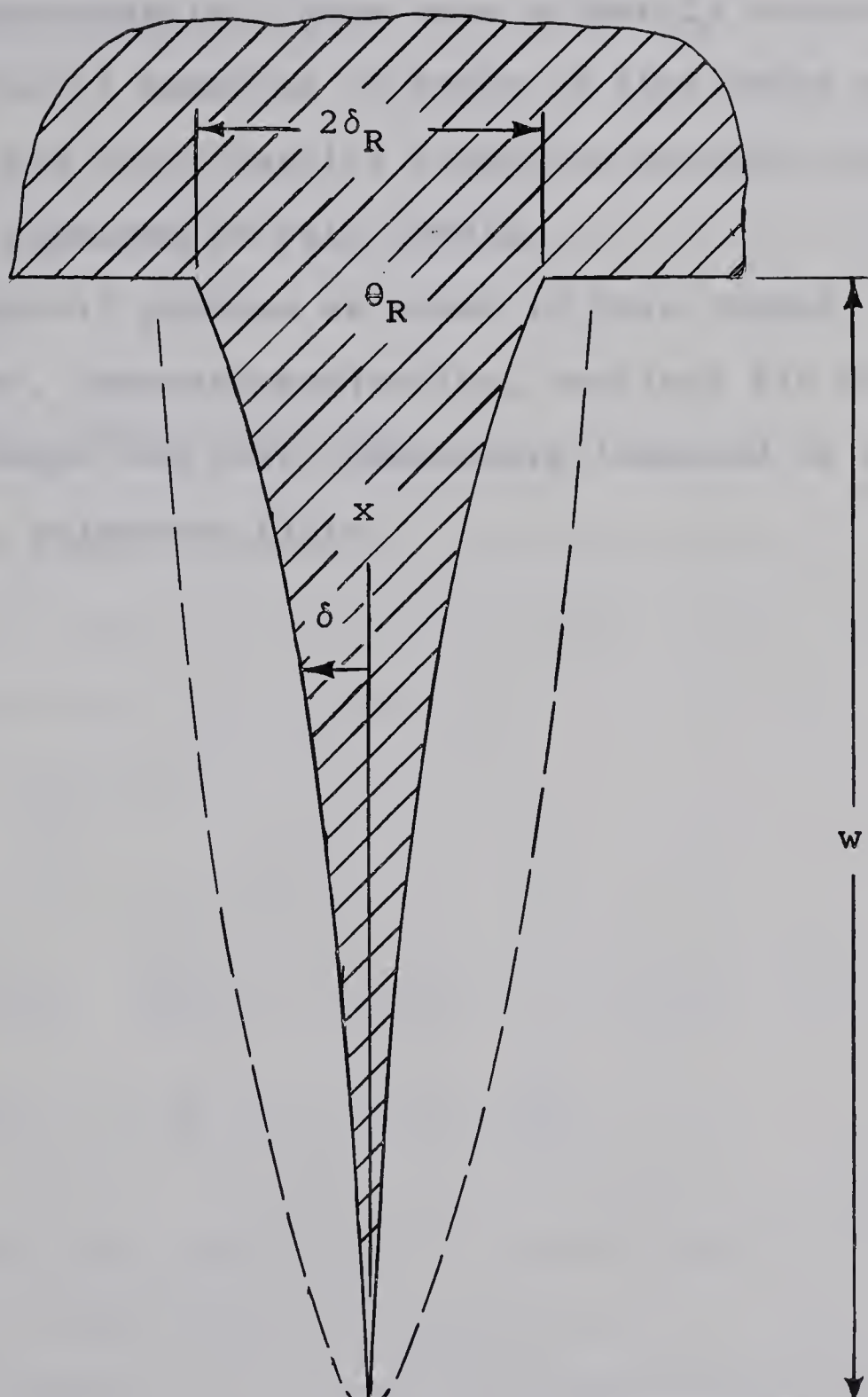
* Numbers designate references given on page 57.

problem is matched to that obtained in the convection problem.

In most practical applications the surface from which heat transfer occurs is nonisothermal. There is a very limited amount of information available in the literature for free convection from a vertical, nonisothermal surface. Sparrow and Gregg [2] give results for the case of uniform heat flux, based on numerical solutions of the differential equations of the boundary layer.

The above authors [3] also considered the power law and exponential forms of surface temperature for the case of gases, i.e., $\sigma \approx 1$.

In the investigation to follow, the problem of conduction through and laminar free convection from a tapered, downward-projecting fin with a large slenderness ratio, w/δ_R , illustrated in figure 1.1, is considered. A large slenderness ratio allows one to neglect the effects of curvature and inclination when solving the flow system as a boundary layer problem. Both theoretical and experimental results for a single fin are presented; in particular for the case in which the fin surface temperature varies in a simple power law form. The effects of slenderness ratio and surrounding fluid were investigated. For the range of conditions considered there was good overall agreement between theory and experiment.



$$\delta = \delta_R (x/w)^m$$

FIG. 1.1 Tapered, Downward-Projecting Fin

Several experimental investigations [4,5,6,7] of free convection from fins have been undertaken in recent years. Unfortunately, these were primarily concerned with the overall behavior of banks of fins under varying conditions and their results cannot be directly compared with those obtained in this thesis.

The overall problem as posed in this thesis, is that of a slender, downward-projecting, vertical fin of known material, shape and root temperature immersed in a given isothermal, quiescent fluid.

CHAPTER II

THEORETICAL ANALYSIS

2.1 BOUNDARY LAYER PROBLEM

An analysis is made for laminar free convection from a downward-projecting fin having a non-uniform surface temperature.

2.1-1 FORMULATION OF PROBLEM

The equations expressing the conservation of mass, momentum and energy for laminar incompressible* flows due to heat conduction from a surface to a fluid in a uniform body force field are:

$$\text{MASS: } \nabla \cdot \tilde{V} = 0$$

$$\text{MOMENTUM: } \frac{D\tilde{V}}{Dt} = -\frac{1}{\rho} \nabla p + \nu \nabla^2 \tilde{V} + \tilde{G} \quad (1)$$

$$\text{ENERGY: } \frac{DT}{Dt} = \kappa \nabla^2 T + \frac{\mathcal{H}}{\rho c_p}$$

Consider the application of these equations to two dimensional steady flow in the semi-infinite region illustrated in figure 1.1. On applying these equations, certain simplifying approximations are made with respect to fluid properties. All properties except density may be taken

* Following Boussinesq.

as constant when dealing with moderate temperature changes [8]. The density is considered as a variable function of temperature only in forming the buoyancy term. The Boussinesqian approximations i.e., $\frac{\rho}{\rho_\infty} \approx 1$ and $\rho - \rho_\infty \neq 0$ are invoked along with the coefficient of expansion, β , defined from the equation of state.

Since it is known a priori that a boundary layer is formed there will be a resulting change in pressure and the sign of this departure from the hydrostatic pressure depends upon whether the fin is being heated or cooled. Taking the pressure as $P = P_s + P_d$, equations (1) may be written as:

$$\begin{aligned} \frac{\partial u}{\partial x} + \frac{\partial v}{\partial y} &= 0 \\ u \frac{\partial u}{\partial x} + v \frac{\partial u}{\partial y} &= - \frac{1}{\rho} \frac{\partial P_d}{\partial x} + v \left(\frac{\partial^2 u}{\partial x^2} + \frac{\partial^2 u}{\partial y^2} \right) + \beta g (T - T_\infty) \quad (2) \\ u \frac{\partial v}{\partial x} + v \frac{\partial v}{\partial y} &= - \frac{1}{\rho} \frac{\partial P_d}{\partial y} + v \left(\frac{\partial^2 v}{\partial x^2} + \frac{\partial^2 v}{\partial y^2} \right) \\ u \frac{\partial T}{\partial x} + v \frac{\partial T}{\partial y} &= \kappa \left(\frac{\partial^2 T}{\partial x^2} + \frac{\partial^2 T}{\partial y^2} \right) + \frac{2v}{c_p} \left[\left(\frac{\partial u}{\partial x} \right)^2 + \left(\frac{\partial v}{\partial y} \right)^2 \right] + \\ &\quad \frac{v}{c_p} \left[\frac{\partial u}{\partial y} + \frac{\partial v}{\partial x} \right]^2 \end{aligned}$$

and are subject to the following boundary conditions:

$$\begin{aligned} y = 0 \quad (x > 0) \quad u = v = 0 \quad T_o = T_o(x) \\ y = \infty \quad u = v = 0 \quad T = T_\infty \end{aligned} \quad (3)$$

In accordance with the usual boundary layer approximations, $y \ll x$, $\frac{\partial}{\partial x} \ll \frac{\partial}{\partial y}$ and hence from the continuity equation $v \ll u$. Using these approximations and neglecting dissipation* a posteriori, equations (2) become**

$$\begin{aligned} \frac{\partial u}{\partial x} + \frac{\partial v}{\partial y} &= 0 \\ u \frac{\partial u}{\partial x} + v \frac{\partial u}{\partial y} &= \beta g(T - T_{\infty}) + v \frac{\partial^2 u}{\partial y^2} \\ u \frac{\partial T}{\partial x} + v \frac{\partial T}{\partial y} &= \kappa \frac{\partial^2 T}{\partial y^2} . \end{aligned} \quad (4)$$

Equations (4) may be written in terms of a stream function, $\psi = \psi(x, y)$ such that $u = \frac{\partial \psi}{\partial y}$ and $v = -\frac{\partial \psi}{\partial x}$, thus satisfying the continuity equation. The velocity components u and v are thus replaced by the derivatives of the stream function and from this substitution there results a pair of partial differential equations for ψ and T as functions of x and y .

$$\begin{aligned} \frac{\partial \psi}{\partial y} \frac{\partial^2 \psi}{\partial x \partial y} - \frac{\partial \psi}{\partial x} \frac{\partial^2 \psi}{\partial y^2} &= \beta g(T - T_{\infty}) + v \frac{\partial^3 \psi}{\partial y^3} \\ \frac{\partial \psi}{\partial y} \frac{\partial T}{\partial x} - \frac{\partial \psi}{\partial x} \frac{\partial T}{\partial y} &= \kappa \frac{\partial^2 T}{\partial y^2} \end{aligned} \quad (5)$$

2.1-2 SIMILARITY SOLUTIONS

It is desirable to seek a similarity transformation which will transform the partial differential equations to

* $0_s = \frac{\beta g w}{c_p} \ll 1$.

** For a complete analysis of reduction of equations see [15].

a pair of ordinary differential equations. Sparrow and Gregg [3] carried out the first similarity analysis for free-convection from non-isothermal surfaces. Yang [9] later did a similar analysis and in both papers the power law and exponential temperature distributions were discussed. It appears [10] that the latter is not really a distinct form and therefore an analysis in which the surface temperature takes the form

$$\theta_o = \theta_R \left(\frac{x}{w} \right)^n \quad (n \geq 0), \quad (\theta = T - T_\infty)$$

will describe the general similarity situation for a fin. This situation is also consistent with a finite temperature at the fin tip equal to that of the surrounding fluid. Therefore, the similarity variables for this case are taken [3] as

$$\psi(x, y) = 4\gamma \left[\frac{\beta g \theta_R}{4\gamma^2 w^n} \right]^{\frac{1}{4}} x^{\frac{n+3}{4}} f(\eta)$$

$$\theta(x, y) = \theta_R \left(\frac{x}{w} \right)^n \phi(\eta) \quad (6)$$

where $\eta = \left[\frac{\beta g \theta_R}{4\gamma^2 w^n} \right]^{\frac{1}{4}} \frac{y}{x^{\frac{1-n}{4}}}$

These variables describe the general case but the resulting ordinary differential equations contain the Prandtl number. A new similarity transformation may be

found which will render the equations independent of Prandtl number. This is done by considering the asymptotic situations of $\sigma \rightarrow 0$ and ∞ . For this analysis the situation of $\sigma \rightarrow \infty$ will be dealt with and will give results which, as well as representing an upper bound, can be expected to lie sufficiently close to the unit Prandtl number results to permit accurate interpolation.

A similar transformation to that utilized by Lefevre [11] for an isothermal surface enables the variables for a non-isothermal surface to be written as

$$\begin{aligned}\psi(x, y) &= 4\kappa \left[\frac{\beta g \theta_R}{4\kappa^2 w^n (1+\sigma)} \right]^{\frac{1}{4}} x^{\frac{n+3}{4}} F(\xi) \\ \theta(x, y) &= \theta_R \left(\frac{x}{w} \right)^n \Phi(\xi)\end{aligned}\quad (7)$$

$$\text{where } \xi = \left[\frac{\beta g \theta_R}{4\kappa^2 w^n (1+\sigma)} \right]^{\frac{1}{4}} \frac{y^{\frac{1-n}{4}}}{x}$$

for the extreme values of Prandtl number.

2.1-3 GOVERNING EQUATIONS

To obtain a set of ordinary differential equations, the similarity variables (7) are substituted in the boundary layer equations (5) to give

$$\sigma \left[F''' + \Phi \right] + (n + 3) FF'' - 2(n + 1)(F')^2 + \Phi = 0 \quad (8)$$

$$\Phi''' + (n + 3) F\Phi' - 4n F' \Phi = 0.$$

These equations become independent of Prandtl number for the extreme values of $\sigma = 0$ and ∞ . In the latter case the momentum equation reduces to $F''' = -\Phi$ and equations (8) reduce to

$$F^V + (n + 3) FF^{IV} - 4n F' F''' = 0 \quad (9)$$

in combined form. The associated boundary conditions are:

$$F(0) = F'(0) = F'''(0) + 1 = 0 \quad (10)$$

$$F'''(\infty) = F'''(\infty) = 0$$

These differ from the unit Prandtl number boundary conditions in just one respect; that is, $F''(\infty) = 0$ replaces $F'(\infty) = 0$ which is regarded as less admissible as $\sigma \rightarrow \infty$.

2.2 SOLUTIONS TO THE BOUNDARY LAYER EQUATIONS

The combined equation (9) may be solved by the method of Meksyn [12,13] which will give the heat transfer and skin friction results. From these results the velocity and temperature distributions may then be determined by a forward integration technique.

2.2-1 MEKSYN'S METHOD

In obtaining solutions to equation (9), use is made of the fact that F''' and F^{IV} are large only in a narrow region close to the fin surface. This fact makes it possible to seek asymptotic solutions of the equations.

Formally solving equation (9) as a linear non-homogeneous first order equation in F^{IV} gives

$$F^{IV} = e^{-H(\xi)} \left[F^{IV}(0) + \int_0^\xi 4n F' F''' e^{H(\xi)} d\xi \right] \quad (11)$$

where

$$H(\xi) = (n + 3) \int F d\xi .$$

A series solution, $F(\xi) = \sum_{r=0}^{\infty} \frac{a_r \xi^r}{r!}$ is now assumed

which allows (11) to be written in the form

$$F^{IV} = e^{-H(\xi)} R(\xi) \quad (12)$$

where $R(\xi) = \sum_{r=0}^{\infty} \frac{b_r \xi^r}{r!}$ (13)

is regarded as a slowly varying function of ξ .

Expanding about the origin in a Maclaurin series and utilizing the differential equation and boundary conditions there, the a_r are readily found in terms of the parameter n and the eigenvalues $F''(0)$ and $F^{IV}(0)$, i.e., α and γ , say. Expansion of (12) and comparison of terms in equal powers of

ξ yield the b_r in terms of the a_r and consequently in terms of n , α and γ . The first few terms of a_r and b_r are:

$$\begin{array}{ll}
 a_0 = 0 & a_5 = 0 \\
 a_1 = 0 & a_6 = -4n\alpha \\
 a_2 = \alpha & a_7 = 4n + (7n - 3)\gamma\alpha \\
 a_3 = -1.0 & a_8 = (3 - 15n)\gamma \\
 a_4 = \gamma &
 \end{array}$$

and

$$\begin{array}{ll}
 b_0 = \gamma & \\
 b_1 = 0 & \\
 b_2 = -4n\alpha & \\
 b_3 = 4n(1 + 2\alpha\gamma) & \\
 b_4 = -16n\gamma & \\
 b_5 = 16n(\gamma^2 - 5n\alpha^2 - 3\alpha^2) & \\
 b_6 = 316n^2\alpha + 220n^2\alpha^2\gamma + 180n\alpha^2\gamma + 180n\alpha &
 \end{array}$$

To facilitate the integration of equation (12), ξ is replaced by a new independent variable τ defined as

$$\tau = H(\xi) = \xi^3 \sum_{r=0}^{\infty} c_r \xi^r$$

where the c_r are found from the expansion of $H(\xi)$ giving the first few terms as:

$$\begin{array}{ll}
 c_0 = \frac{(n + 3) a_2}{3!} & c_4 = \frac{(n + 3) a_6}{7!} \\
 c_1 = \frac{(n + 3) a_3}{4!} & c_5 = \frac{(n + 3) a_7}{8!}
 \end{array}$$

$$c_2 = \frac{(n+3) a_4}{5!} \quad c_6 = \frac{(n+3) a_8}{9!}$$

$$c_3 = 0$$

It is now necessary to express ξ in terms of τ by inverting the series for τ , taking

$$\xi = \sum_{s=0}^{\infty} \frac{A_s \tau^{(s+1)/3}}{s+1} \quad (14)$$

which is valid for sufficiently small values of τ . Following [12], A_s is the coefficient of ξ^s in the expression

$$(c_0 + c_1 \xi + c_2 \xi^2 + c_3 \xi^3 + \dots)^{-(s+1)/3}$$

giving

$$A_0 = c_0^{-1/3} \quad A_1 = -\frac{2}{3} c_1 c_0^{-5/3}$$

$$A_2 = \frac{c_1^2}{c_0^3} - \frac{c_2}{c_0^2}$$

$$A_3 = c_0^{-4/3} \left[\frac{28}{9} \frac{c_1 c_2}{c_0^2} - \frac{140}{81} \left(\frac{c_1}{c_0} \right)^3 \right]$$

$$A_4 = c_0^{-5/3} \left[-\frac{5}{3} \frac{c_4}{c_0} + \frac{20}{9} \left(\frac{c_2}{c_0} \right)^2 - \frac{220}{27} \frac{c_1^2 c_2}{c_0^3} + \frac{770}{243} \left(\frac{c_1}{c_0} \right)^4 \right]$$

etc.

The A_s , through the c_r and hence the a_r , implicitly involve n , α and γ .

Formally integrating equation (12) once and using the boundary condition at the origin on F''' gives

$$F''' = \int_0^\tau e^{-\tau} R(\xi) \frac{d\xi}{d\tau} d\tau - 1. \quad (15)$$

Utilizing equations (13) and (14) and re-writing $R(\xi) \frac{d\xi}{d\tau}$

as

$$R(\xi) \frac{d\xi}{d\tau} = \tau^{-2/3} \sum_{s=0}^{\infty} d_s \tau^{s/3} \quad (16)$$

where $3d_s$ is the coefficient of ξ^s in

$$\left(b_0 + b_1 \xi + \frac{b_2 \xi^2}{2!} + \frac{b_3 \xi^3}{3!} + \dots \right) \left(c_0 + c_1 \xi + c_2 \xi^2 + c_3 \xi^3 + \dots \right)^{\frac{-(s+1)}{3}}$$

gives

$$d_0 = \frac{1}{3} c_0^{-1/3} b_0$$

$$d_1 = \frac{1}{3} c_0^{-2/3} \left[b_1 - \frac{2}{3} b_0 \frac{c_1}{c_0} \right]$$

$$d_2 = \frac{1}{3} c_0^{-1} \left[\frac{b_2}{2} - \frac{b_1 c_1}{c_0} - b_0 \frac{c_2}{c_0} + b_0 \left(\frac{c_1}{c_0} \right)^2 \right]$$

etc.*

Substituting (16) in (15), we obtain

$$F''' = \sum_{s=0}^{\infty} d_s \int_0^\tau e^{-\tau} \tau^{(s+1)/3} - 1 d\tau - 1,$$

so that the condition $F'''(\infty) = 0$ is satisfied if

$$\sum_{s=0}^{\infty} d_s \Gamma \left(\frac{s+1}{3} \right) = 1. \quad (17)$$

* For brevity and due to their complexity the remaining coefficients, d_s , are omitted here. They are given in the computer program in Appendix A, p. 59.

This series gives only one equation for the eigenvalues α and γ in terms of the parameter n and therefore a second equation is required. This second equation is obtained by satisfying the condition $F'''(\infty) = 0$ in a similar manner by letting $F'''(\xi) = e^{-H(\xi)} Q(\xi)$ and proceeding as above. $Q(\xi)$ results in a new set of values, b'_r , the first few being

$$\begin{aligned} b'_0 &= -1 \\ b'_1 &= \gamma \\ b'_2 &= 0 \\ b'_3 &= -\alpha(5n + 3) \\ b'_4 &= 5n + 3 + \alpha\gamma(11n + 9) \\ b'_5 &= -\gamma(21n + 15) \\ b'_6 &= 21n\gamma^2 + 15\gamma^2 - 130n^2\alpha^2 - 228n\alpha^2 - 90\alpha^2 \end{aligned}$$

The a_r , c_r and A_s terms are as previously obtained and the d_s are replaced by g_s which incorporate the new values b'_r . This results in

$$-\alpha = \sum_{s=0}^{\infty} g_s \Gamma\left(\frac{s+1}{3}\right), \quad (18)$$

where the g_s , like the d_s , contain α , γ and the temperature index n . Therefore equations (17) and (18) contain the two unknown eigenvalues and constitute the essential solution of the problem.

2.2-2 SOLUTION FOR EIGENVALUES

Since the simultaneous equations (17) and (18) contain α and γ implicitly it is convenient to solve them numerically by an iterative procedure, following truncation after seven terms. This procedure was carried out by a computer program as given in Appendix A, written in Fortran IV language. The calculations were carried out on an IBM 7040-1401 machine in the Department of Computing Science, University of Alberta.

The basic procedure involved in the program is given as follows. The program was initially set up for seven terms in each of the series. With the temperature index $n = 0$, an initial value of both α and γ was assumed. Each series was then summed and checked with the correct sum, i.e., unity for equation (17) and $-\alpha$ for equation (18). If these sums were not within the set limit of their correct value, α was incremented by an amount proportional to the error in one series while γ was held constant. Using the new value of α the series were again summed and if found to be still in error, γ was incremented by an amount proportional to the error in the second series while α was held constant. This iterative procedure was repeated until the two series came within the set limit of their correct sum thus producing acceptable values of α and γ for $n = 0$. The

procedure was repeated for the range of values of n from 0 to 3 in increments of 0.1. In each case the initial estimates of α and γ used to begin the iterative procedure were those accepted for the previous value of n .

In summing each of the series (17) and (18) frequent use was made of Euler's transformation to remove divergence when necessary. Since many summations were required in the iterative process it was necessary to adopt a systematic application of the Euler transformation: this was incorporated in a subroutine to the main program.

When the series exhibited divergence, the transformation was begun at the first term but additional transformations, each starting with a progressively higher term were also carried out. If none of the resulting series were convergent the process was repeated on the first transformation. However, if one or more of the first set of transformations gave convergence the series with the smallest last term was used in the analysis, which then proceeded in the iterative process. In the majority of cases the series chosen in this manner also resulted in the series with the largest number of unchanged terms.

The eigenvalues α and γ thus obtained are plotted versus n in figure 2.1 together with the corresponding values of γ for $\sigma = 1$ [3] and the extreme values of γ obtained by other authors.

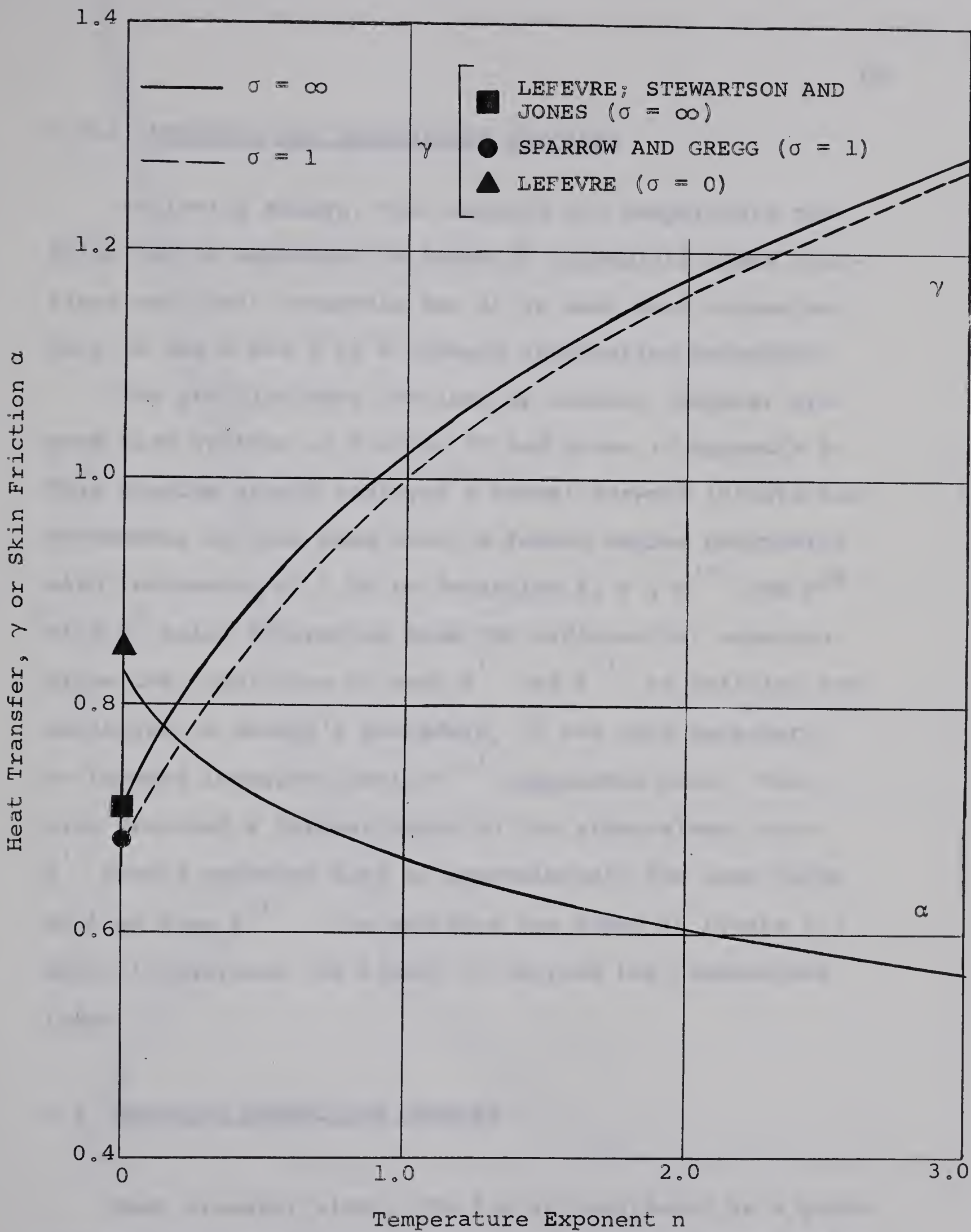


Fig. 2.1 Heat Transfer and Skin Friction Results

2.2-3 VELOCITY AND TEMPERATURE PROFILES

Following Meksyn, the velocity and temperature profiles can be expressed in terms of incomplete gamma functions and their integrals but it is much more convenient here to use α and γ in a forward integration procedure.

The profiles were obtained by another computer program also written in Fortran IV and given in Appendix B. This program simply employed a normal forward integration procedure, in this case using a fourth degree polynomial with increments of 0.05 to determine F , F' , F''' and F^{IV} with F^V being determined from the differential equation. Since the conditions on both F'' and F''' at infinity are satisfied in Meksyn's procedure, it was only necessary to forward integrate until F''' approached zero. This also provided a further check on the eigenvalues since F'' should approach zero at approximately the same value of ξ as does F''' . The profiles are shown in figure 2.2 which illustrates the effect of varying the temperature index.

2.3 MATCHING CONDUCTION PROBLEM

Heat transfer within the fin is considered as a quasi-one-dimensional conduction problem with the heat transfer coefficient and temperature at the fin surface varying in

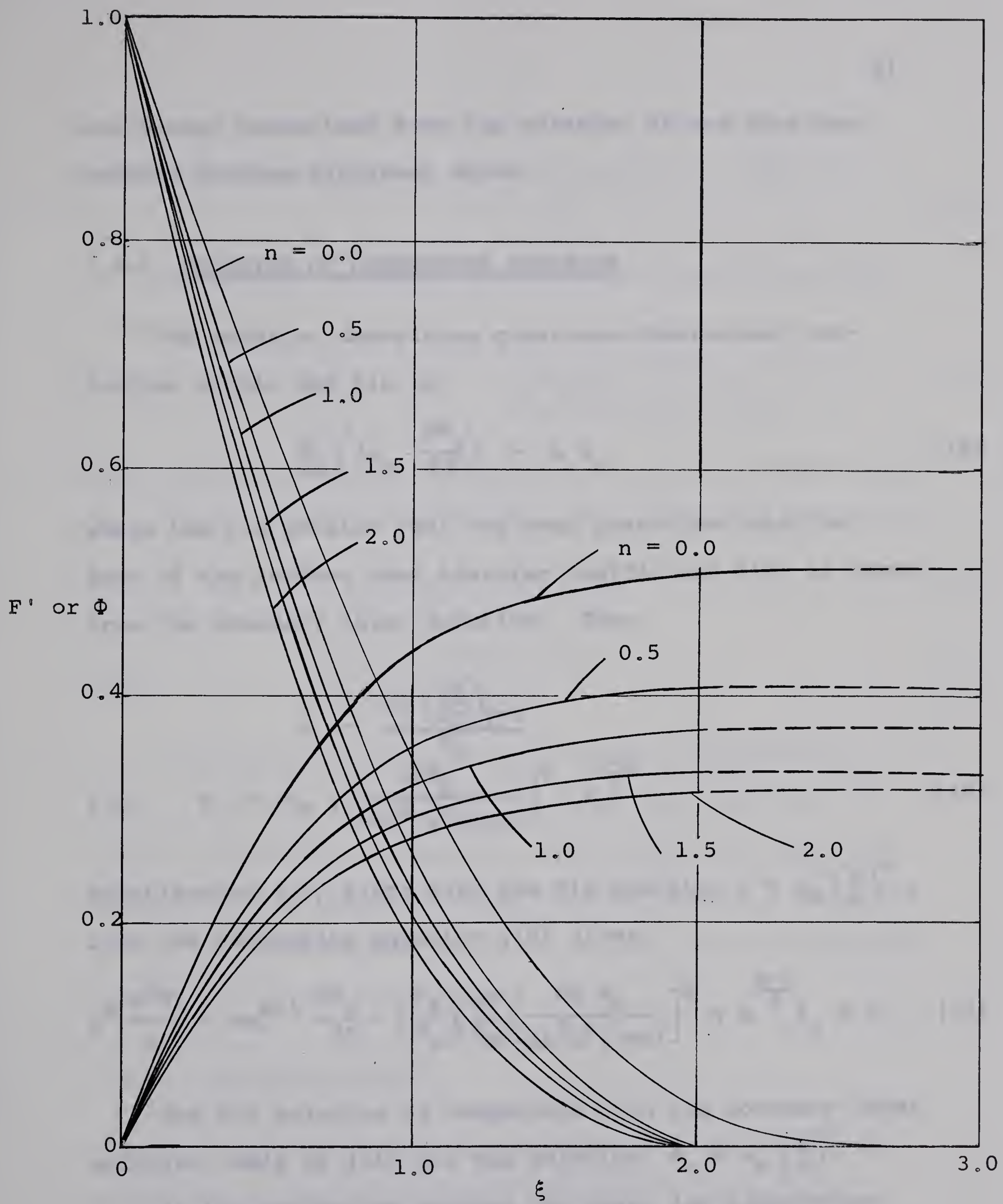


FIG. 2.2 Velocity and Temperature Profiles

the manner prescribed from the solution of the free convection problem discussed above.

2.3-1 SOLUTION OF CONDUCTION EQUATION

The equation describing quasi-one-dimensional conduction within the fin is

$$\frac{d}{dx} \left(\delta k_s \frac{d\theta_o}{dx} \right) = h \theta_o \quad (19)$$

where the fin profile $\delta(x)$ has been prescribed and the form of the surface heat transfer coefficient $h(x)$ is known from the boundary layer solution. Thus

$$h = \frac{k_f \left(\frac{\partial \theta}{\partial y} \right)_{y=0}}{\theta_o}$$

i.e. $h = k_f \gamma \left[\frac{\beta g \theta_R}{4 \kappa^2 w^n (1+\sigma)} \right]^{\frac{1}{4}} x^{\frac{n-1}{4}}$. (20)

Substituting (20) along with the fin profile, $\delta = \delta_R \left(\frac{x}{w} \right)^m$, into the conduction equation (19) gives

$$x^m \frac{d^2 \theta_o}{dx^2} + mx^{m-1} \frac{d\theta_o}{dx} - \left(\frac{k_f}{k_s} \right) \left(\frac{w^m}{\delta_R} \right) \left[\frac{\beta g \theta_R}{4 \kappa^2 w^n (1+\sigma)} \right]^{\frac{1}{4}} \gamma x^{\frac{n-1}{4}} \theta_o = 0 . \quad (21)$$

The fin solution is compatible with the boundary layer solution, only if (21) has the solution $\theta_o = \theta_R \left(\frac{x}{w} \right)^n$.

In the conduction problem any power law temperature solution requires that the exponent of x in the coefficient

of the second derivative is two greater than that of the corresponding coefficient of the function θ_0 . That is,

$$n = 4m - 7. \quad (22)$$

The indicial equation gives another relation between n and m ; i.e.

$$n = \frac{1}{2}(1 - m) + \frac{1}{2} \left\{ (m - 1)^2 + 4 \left(\frac{k_f}{k_s} \right) \left(\frac{w^m}{\delta_R} \right) \left[\frac{\beta g \theta_R}{4 \kappa^2 w^n (1+\sigma)} \right]^{\frac{1}{4}} \gamma \right\}^{\frac{1}{2}} \quad (23)$$

where the positive root is taken to satisfy the requirement that $n > 0$. The elimination of m from (22) and (23) results in

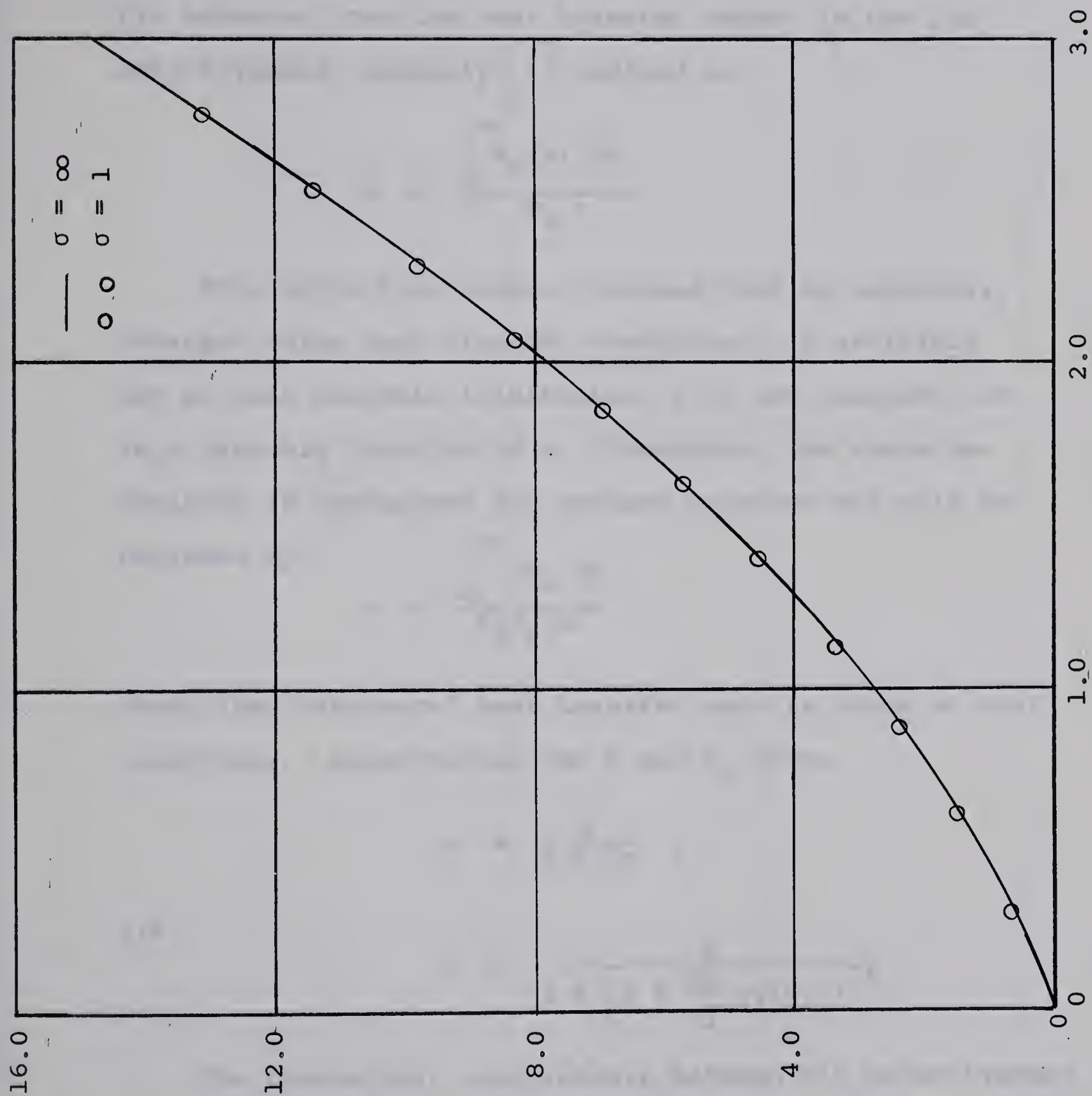
$$n = -\frac{3}{10} + \frac{1}{10} \left[9 + \frac{80}{\sqrt{2}} \chi \gamma \right]^{\frac{1}{2}} \quad (24)$$

$$\text{where } \chi = \left(\frac{k_f}{k_s} \right) \left(\frac{w}{\delta_R} \right) \left[\frac{\beta g \theta_R w^3}{\kappa^2 (1+\sigma)} \right]^{\frac{1}{4}}. \quad (25)$$

Thus there is only one value of the dimensionless group χ for each value of n , for which the power law fin surface temperature profile is valid within the approximations of this analysis. The relation between n and χ for $\sigma = \infty$ is illustrated in figure 2.3 along with corresponding theoretical points for $\sigma = 1$.

2.3-2 FIN EFFECTIVENESS

Although equation (24) gives the solution to the fin conduction problem in terms of temperature index n , it does not fully describe the heat transfer characteristics



$$X = \left(\frac{k_f}{k_s} \right) \left(\frac{w}{\rho R} \right)^{1/4} \left[\frac{B g \theta R}{k^2 (1+\alpha)} \right]$$

FIG. 2.3 -Determination of Temperature Index

of the fin itself. The quantity that best describes the fin behavior from the heat transfer aspect is the fin effectiveness, normally [1] defined as

$$\epsilon = \frac{\int_0^W \theta_o(x) dx}{\theta_R w} .$$

This definition however assumes that an empirical, constant value heat transfer coefficient is available but as this analysis illustrates, h is not constant but is a variable function of x . Therefore, the above definition is inadequate for present purposes and will be replaced by

$$\epsilon = \frac{\int_0^W h \theta_o dx}{h_R \theta_R w} ,$$

where the "reference" heat transfer rate is taken at root conditions. Substituting for h and θ_o gives

$$\epsilon = \frac{4}{3 + 5n} ,$$

i.e.

$$\epsilon = \frac{8}{3 + \left[9 + \frac{80}{\sqrt{2}} \chi \gamma(n, \sigma) \right]^{\frac{1}{2}}} \quad (26)$$

The theoretical relationship between fin effectiveness ϵ and the non-dimensional group χ is shown in figure 2.4 for the cases of $\sigma = \infty$ and 1.

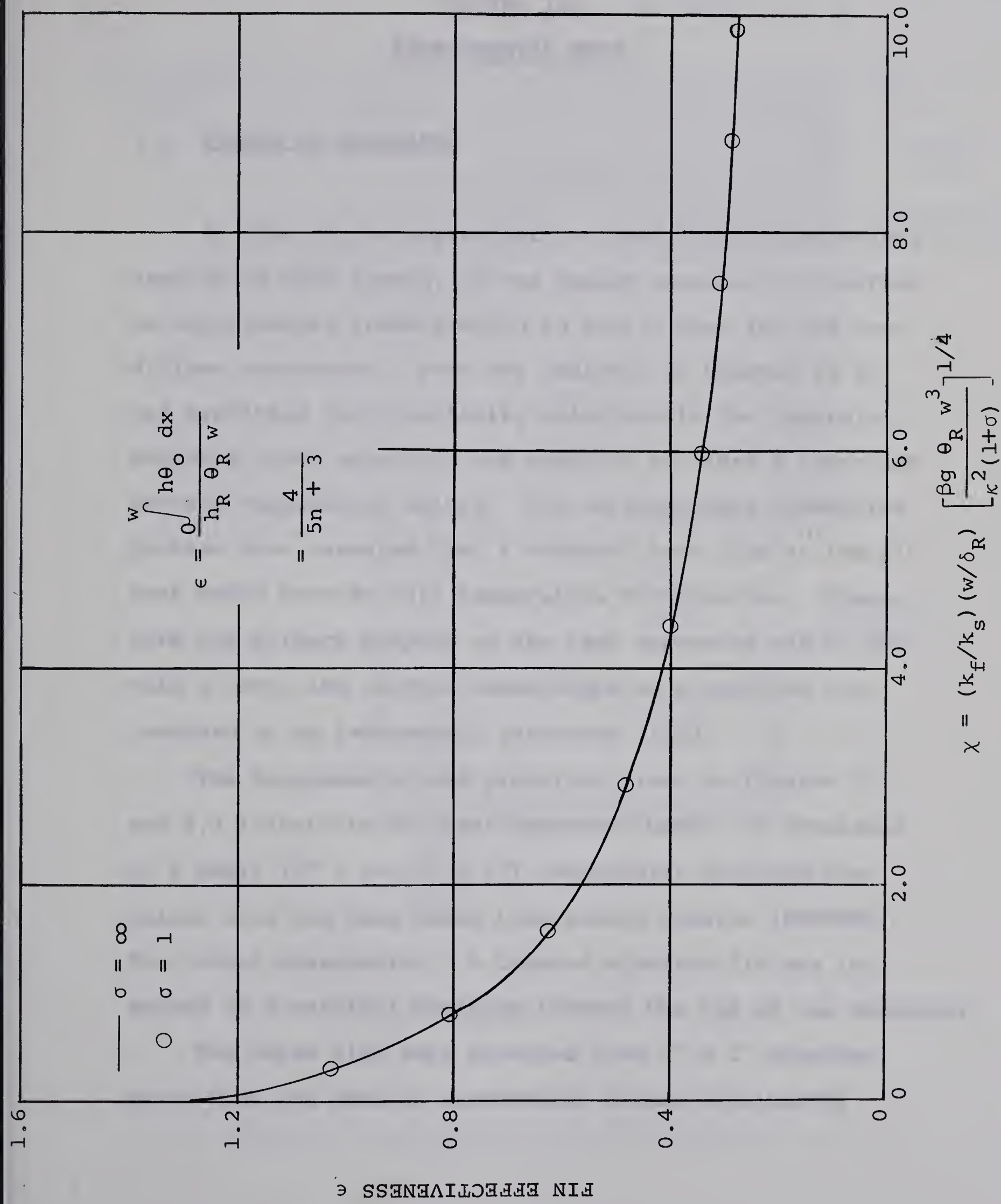


FIG. 2.4 Fin Effectiveness

CHAPTER III

EXPERIMENTAL WORK

3.1 DESIGN OF APPARATUS

In view of the approximations used in the theoretical section of this thesis, it was deemed necessary to perform an experimental investigation to verify them for the conditions considered. From the analysis of Chapter II it was predicted that similarity solutions to the governing boundary layer equations are possible provided a power law surface temperature exists. The corresponding conduction problem also revealed that a constant heat flux at the fin root would provide this temperature distribution. Therefore the primary purpose of the test apparatus was to obtain a power law surface temperature on a vertical fin immersed in an isothermal, quiescent fluid.

The diagrammatic and pictorial views in figures 3.1 and 3.2 illustrate the test apparatus used. It consisted of a small (5" x 6-1/2" x 8") rectangular aluminum container with one face being transparent plastic (PERSPEX) for visual observation. A tapered aluminum fin was inserted in a vertical position through the top of the container.

The three fins were produced from 4" x 1" aluminum plate with the various slenderness ratios obtained by

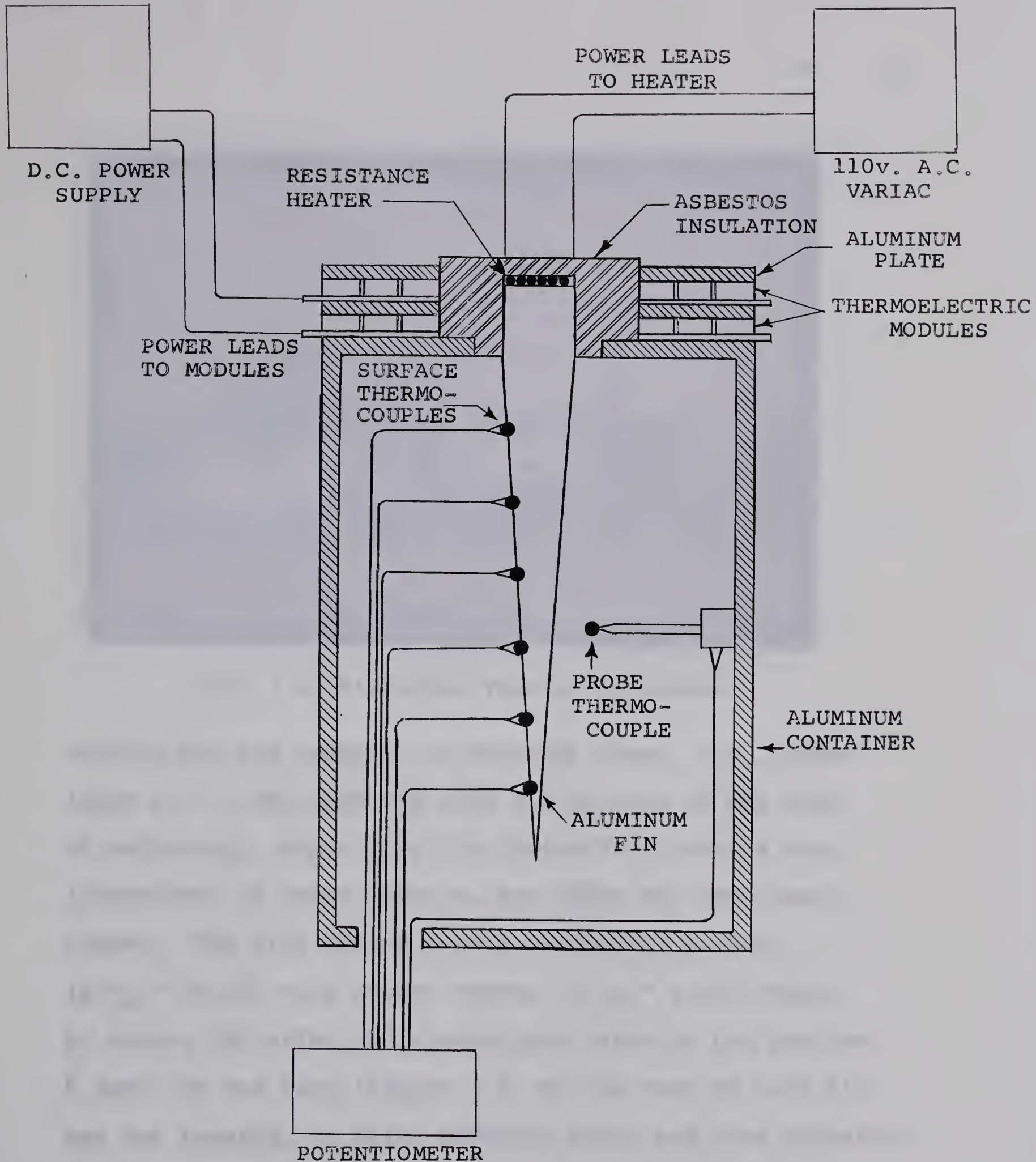


FIG. 3.1 Diagrammatic View of Apparatus

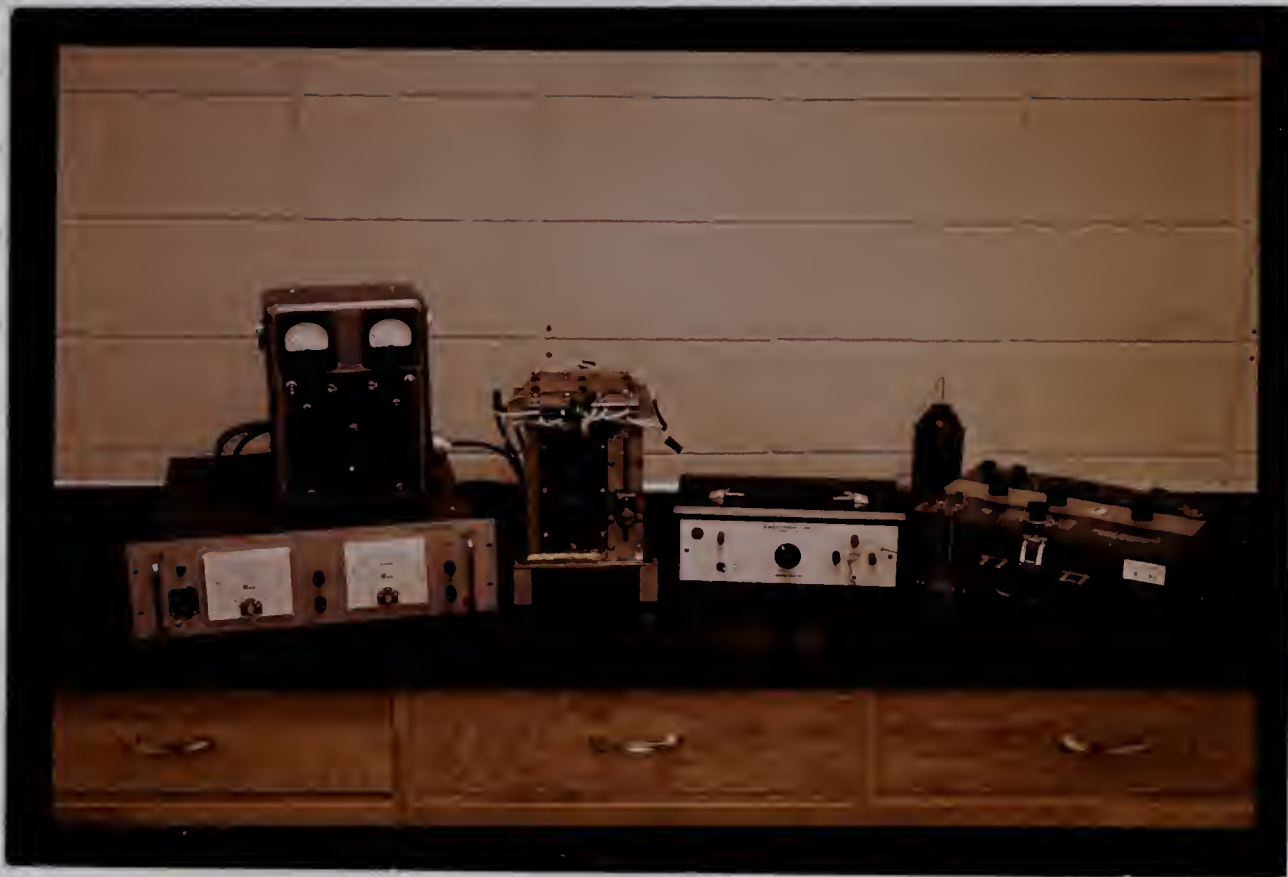


FIG. 3.2 Pictorial View of Apparatus

varying the fin lengths. A straight taper, i.e., shape index $m = 1$, was used for each fin because of the ease of machining. Also, since the theoretical results are independent of shape index m , any shape may have been chosen. The fins varied from a relatively slender ($w/\delta_R = 14.22$) to a rather stubby ($w/\delta_R = 6.15$) shape to reveal the effect of slenderness ratio on the problem. A depth of one inch (figure 3.1) at the root of each fin was not tapered, to allow mounting space and thus allowing only the tapered portion to be immersed in the fluid.

The root heating of each fin was achieved by cementing strands of #31 (0.0089" diameter) Greening 60-15

high resistance (8.25 ohms/ft.) nickel-chromium wire on the root as shown in figure 3.1. The cement used for this purpose was BUDD HT (GA-100) high temperature ceramic cement. This type of heater along with the one inch untapered portion at the fin root was considered to give a constant uniform heat flux at the beginning of the fin taper. The heaters used had a capacity of approximately 200 watts at 110v A.C. A variac was used to supply the power to the heaters so as to obtain a wide range of heater input. To reduce heat losses and practically eliminate heat transfer from the fin to the box, the fin root was completely enclosed with asbestos as illustrated in figure 3.1.

Since the problem under consideration is steady state it was necessary to have a method of cooling the ascending boundary layers to obtain an equilibrium condition. It was thought that thermoelectric methods would give fine control and consequently twelve thermoelectric cooling modules were used. The Frigistor modules used are rated at 22.2 watts for a maximum current of thirty amperes when the hot face is held at 27°C and the cold face is thermally insulated. There is an electrically insulating film on both sides to avoid electrical short circuits.

These modules were mounted on the aluminum container

on either side of the fin root as shown in figure 3.1. Due to space limitations it was necessary to pyramid the modules with two layers of three modules on each side. These twelve modules were then connected in series and the power supplied by a Hewlett Packard D.C. power supply rated at forty-five amperes and eighteen volts. Since the modules require an adequate heat sink in order to cool properly, a 1/4" aluminum plate was placed over each layer of modules. The modules operate on relatively small temperature differences between "hot" and "cold" sides and since the "hot" side cannot be higher than 100°C a blower was used to cool the aluminum plates.

3.2 INSTRUMENTATION

From the theoretical analysis, all results depend upon the temperature index n and therefore it was necessary to obtain a tolerably accurate value of this experimentally. Temperature readings were therefore required at several positions along the fin surface. Embedding several evenly-spaced thermocouples along one face of the fin accomplished this. The grooves were cut laterally across the surface such that the individual thermocouple wires were led out along isotherms. The depth was just sufficient to allow the thermocouples to be flush with the

surface when bonded in place with epoxy glue. Honeywell Type-J iron-constantan (0.010 inch diameter) butt welded thermocouples were used throughout the test apparatus.

Temperature profiles in the boundary layer adjacent to the fin surface were obtained with a probe thermocouple. For convenience and ease of locating the probe near the fin surface, the wires at the measuring junction were brought to a blunt point. In comparing readings with this probe and an "isothermal junction" probe, there were no appreciable differences found; thus conduction errors appear to have been tolerably small.

The remaining thermocouples were used to obtain a bulk fluid temperature. Since it was not known if an isothermal fluid could be attained, several thermocouples were located throughout the fluid. These were all located approximately 1/2" from the inside surface of the container.

All of the above-mentioned thermocouples were connected to a switching unit whose single output was measured with a potentiometer. To reduce errors in thermocouple readings, an ice bath was used as the reference point.

3.3 EXPERIMENTAL METHOD

The theoretical prediction that all results are dependent upon one non-dimensional group, χ , suggested that

the tests be designed to verify this over a range of conditions of practical interest.

3.3-1 TESTING PROGRAM

The experimental work was carried out in three phases. The first investigations were carried out to test the validity of the n versus χ relationship. The non-dimensional group χ consists of three separate, non-dimensional groups; namely the conductivity ratio, the slenderness ratio and a variable Prandtl-Grashof number. Two values of the conductivity ratio were obtained by using both water and glycerine as the bulk fluids: this would also give an indication of any independent effect of Prandtl number. The effect of variations in slenderness ratio was studied by using the three different fins previously mentioned. Variations in the Prandtl-Grashof number, other than by using two different fluids, were achieved by changing the root temperature of the fin.

Temperature profiles in the boundary layer adjacent to the fin surface were measured to verify the profiles obtained in Chapter II. Four profiles were measured, two each in water and glycerine for one fin ($w/\delta_R = 14.22$). These were obtained at various positions along the fin surface in order to check the validity of the similarity transformations.

The last phase of the experimental analysis was obtaining photographs of the boundary layer for two ranges of the temperature index n . To obtain these a fin was mounted in a transparent plastic (PERSPEX) tank which was then placed in a Schlieren apparatus modified to operate as a shadowgraph. The purpose of these tests was to examine the shape of the boundary layer and heat flux curve for $n < 0.2$ and $n > 1$.

3.3-2 PRELIMINARY TESTS

In the early stages of the experimental work several trial runs were made to check the operation of the apparatus. From these it was found that very slight variations in surface thermocouple readings made it extremely difficult to establish a reliable value of the temperature index n . Due to the method used in manufacturing the thermocouples it was deemed necessary to calibrate them all. These were calibrated at both the freezing and boiling points of water and only those with errors of less than 0.1°F were used.

During the calibration of the thermocouples it was noted that very small temperature gradients across the switching unit would give false readings in the thermocouples. This difficulty was eliminated by covering the switching unit with a cardboard box to maintain isothermal

conditions around the unit.

Preliminary tests performed in water showed very erratic readings in most thermocouples. This was attributed to electrical conduction through the water and was eliminated by coating the immersed portion of all thermocouples with a clear acrylic spray.

3.3-3 TEST PROCEDURE

Considering first the procedure used in obtaining the experimental n versus χ relationship, the following steps were taken. With the fin, container and fluid initially at room temperature all thermocouple readings were recorded. If any were in appreciable disagreement with the others and it was thought to be due to malfunctioning of those thermocouples for some particular reason, they were disregarded for the remainder of the test. Power was then supplied to the modules which were allowed to operate for a short period of time to cool the fluid slightly before the fin heater was turned on. This method was found to reduce the time required to obtain steady state conditions.

After the heater had been switched to a prescribed power setting and allowed to operate for 10 - 15 minutes the power to the modules was regulated until there was no appreciable change in the thermocouple readings over a

10 - 15 minute interval. Once steady-state conditions had been attained all thermocouple readings were recorded: the power to the heater was then changed and the procedure repeated.

In obtaining boundary layer temperature profiles there was only one additional step required to those given above. After steady state conditions had been reached and thermocouple readings taken, the probe was positioned as accurately as possible at the fin surface at a particular distance from the fin tip. Probe readings were then taken for equal increments of distance proceeding from the fin surface to the outer region of the thermal boundary layer.

The visual tests consisted of setting up the fin and plastic tank in the Schlieren apparatus and applying the appropriate power to obtain the desired value of temperature index n . As before, the value of n was determined from the fin surface temperatures and the bulk fluid temperature. Photographs were then taken of the corresponding boundary layers and heat flux curves as seen on the screen.

CHAPTER IV
DISCUSSION OF RESULTS

4.1 HEAT TRANSFER AND SKIN FRICTION

The eigenvalues as shown in figure 2.1 were obtained using seven terms in each of the two infinite series. To note the effect of the number of terms in the series, the eigenvalues were also obtained using 4, 5 and 6 terms. Maximum variation in the results for all four cases was found to be less than 5 percent. Also, variations in the values for six and seven terms were of the order of 1%, indicating that seven terms are sufficient for practical purposes and give more accurate results than in similar work [13].

The predominant effects of n on the heat transfer and skin friction results, for the range of n considered, is clearly shown in figure 2.1. It is evident that increasing n causes a steepening of the temperature profile and similarly it suggests a monotonically decreasing tendency for the velocity profile. Whether these trends would continue for larger values of n cannot be established from the results shown.

The independent effect of Prandtl number on any particular fin temperature distribution appears quite slight since figure 2.1 reveals only a small change in heat

transfer between $\sigma = 1$ and ∞ over the range of n considered. This tends to suggest that interpolation in the range $1 \leq \sigma \leq \infty$, i.e., for non-metallic liquids, should be accurate. Tolerably accurate extrapolation into the gaseous region, $\sigma \lesssim 1$, is also reasonable to expect. It therefore appears that the independent effect of Prandtl number not contained in the variable Prandtl-Grashof number is quite small over a large range of Prandtl numbers. Lefevre's results [11] for an isothermal plate suggest that $\gamma(n, \sigma)$ is more dependent on n than σ . From [11], $\gamma(0, \infty) = 0.711$ and $\gamma(0, 0) = 0.849$. Therefore, results presented here appear to apply for all but the smallest Prandtl numbers, which correspond to the liquid metals.

The neglect of the dissipation terms is justified since the Ostrach number, 0_s , is of the order of 10^{-6} .

4.2 TEMPERATURE INDEX

Perhaps the single most significant result to arise from the theoretical analysis is the n versus χ relationship given by equation (24). From this it is seen that the temperature index is a function of three non-dimensional groups, namely, k_f/k_s , w/δ_R , $\beta g \theta_R w^3/\kappa^2(1+\sigma)$ as well as the heat transfer rate, γ , at the fin surface. The conductivity ratio reflects the effect of conduction through an interface between two different conducting media. The

slenderness ratio reveals perhaps one of the most surprising results - that the fin temperature distribution depends on overall geometry as opposed to the precise form of the fin profile. The group $\beta g \theta_R w^3 / \kappa^2 (1+\sigma)$ results from the Lefevre-type transformation and may be taken as a generalized "driving potential". This group, unlike the Grashof or Rayleigh numbers, completely specifies conditions over the entire Prandtl number range. It becomes $\sigma^2 Gr$ as $\sigma \rightarrow 0$ and σGr as $\sigma \rightarrow \infty$, both of which are known to be the correct forms of the "driving potential" for these extreme values of σ .

The theoretical $n - \chi$ relation in figure 2.3 for the range $0 \leq n \leq 3.0$ illustrates the effective independence of Prandtl number in the range $1 \leq \sigma \leq \infty$. This independence implies that the results will at least be accurate for all non-metallic fluids. Table I is a summary of test results from which values of χ were calculated. The corresponding experimental values of the temperature index n were obtained from the slope of a log-log plot of surface temperature versus dimensionless distance along the fin surface. The root temperature was calculated by extrapolation to the root according to these values of temperature and temperature index. A sample calculation of the conversion of thermocouple readings may be found in Appendix C.

Slenderness Ratio (w/δ_R)	14.22		10.63		6.15	
Conductivity Ratio (k_f/k_s)	.00264	.00125	.00261	.00124	.00265	.00124
Non-dimensional Temperature $\left(\frac{\beta g \theta_R w^3}{\kappa^2 (1+\sigma)}\right) \times 10^{-6}$	166.5	5.61	74.3	1.86	14.1	1.17
	171.5	1.06	52.8	3.0	18.2	0.95
	159	1.33	96	1.09	25	0.184
	156.5	1.06	161	3.83	35	0.57
	162.5	2.43	23.7	4.15	92.2	-
	165.5	-	-	-	-	-

TABLE I

SUMMARY OF TEST RESULTS

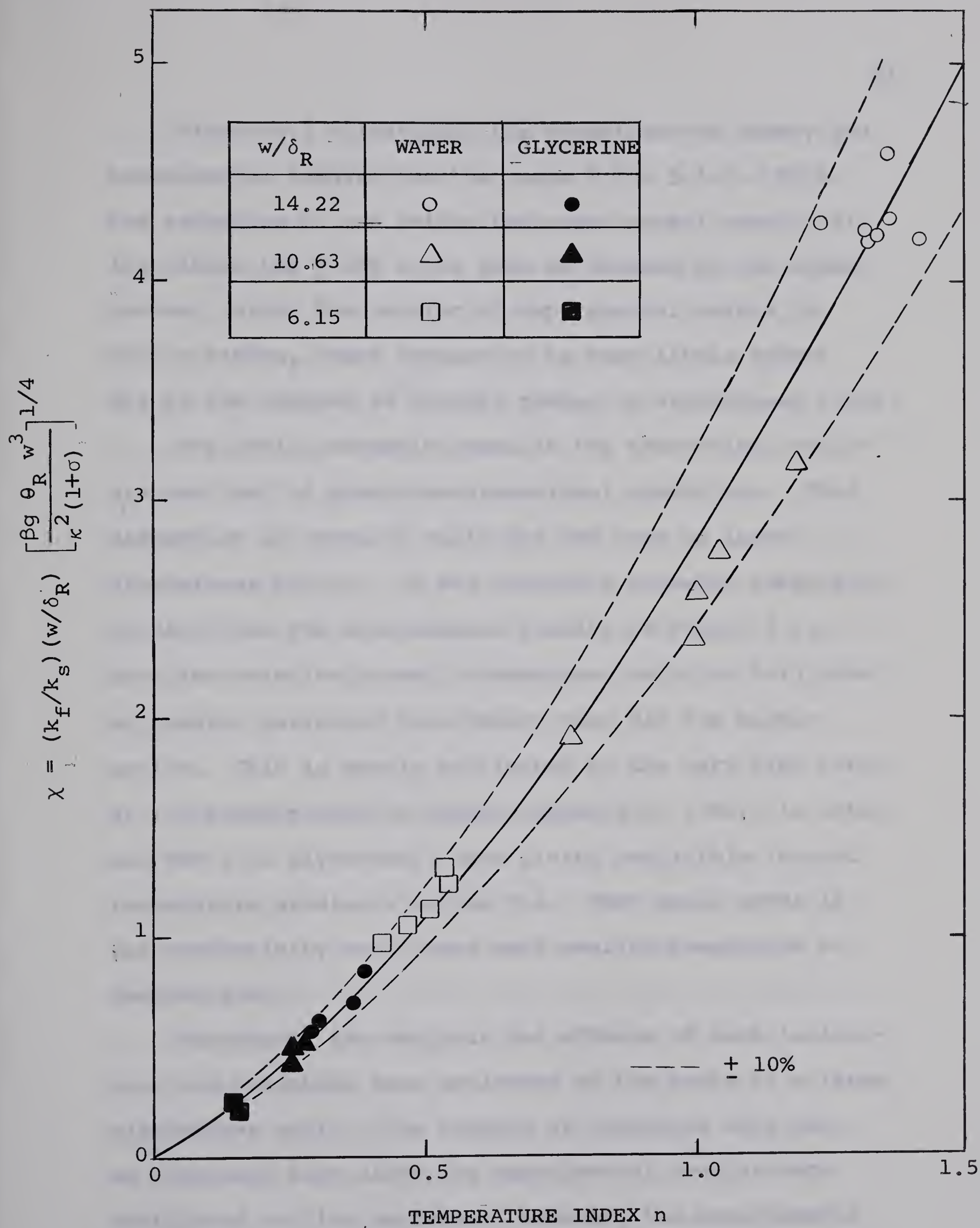
FIG. 4.1 Comparison of $n - \chi$ Relation

Figure 4.1 illustrates the comparison of theory and experimental results for the range $0 \leq n \leq 1.5$. With the exception of two points the experimental results all lie within the $\pm 10\%$ error band as denoted by the broken curves. Since the scatter of experimental points is fairly random, there appears to be very little effect due to the changes in Prandtl number or slenderness ratio.

One basic assumption made in the theoretical analysis was that of quasi-one-dimensional conduction. This assumption is normally valid for the case of large slenderness ratios. It was therefore somewhat surprising to find from the experimental results of figure 4.1, that the relatively small slenderness ratio of 6.15 gave no greater deviation from theory than did the higher ratios. This is mainly attributed to the very high ratio of fin conductivity to fluid conductivity (380:1 in water and 800:1 in glycerine), thus giving negligible lateral temperature gradients in the fin. What would occur if the conductivity ratio were much smaller remains to be demonstrated.

Throughout the analysis the effects of both inclination and curvature were neglected on the basis of a large slenderness ratio. The effects of curvature will not be discussed here since the experimental results were restricted to flat surfaces. However, the experimental

analysis did involve inclination. If taken into account, the main contribution due to inclination will occur in the x-momentum equation in which the buoyancy term is replaced by $\beta g \cos \lambda (T - T_{\infty})$, where the fin half angle, λ , is obtained from the expression $\delta_R/w = \tan \lambda$. The additional term, $\cos \lambda$, would occur throughout the analysis as $(\cos \lambda)^{1/4}$. Considering the smallest slenderness ratio ($w/\delta_R = 6.15$) tested, λ is $9^\circ 14'$ and $(\cos \lambda)^{1/4} = 0.9967$, thus introducing an error of only 0.325%. Therefore it appears, as the experimental results demonstrate, that for practical cases the effects of inclination are negligible. It is probable that the assumption of quasi-one-dimensional conduction will be violated before inclination has any significant effect.

4.3 VELOCITY AND TEMPERATURE PROFILES

The theoretical velocity and temperature profiles in the boundary layer as obtained in Chapter II are shown in figure 2.2. These profiles reveal the familiar characteristics of a large Prandtl number system in which the momentum boundary layer extends beyond the thermal boundary layer. Due to the boundary conditions for this system the temperature profile is contained between the heated fin surface and the velocity maximum.

Utilizing the Lefevre-type transformation as $\sigma \rightarrow \infty$ results in the neglect of the inertia terms but not the corresponding advective* terms in the energy equation. Therefore the profiles represent the solution, within the thermal boundary layer, of the complete energy equation together with a reduced momentum equation.

The velocity profiles were not determined beyond the thermal boundary layer. However, it is possible to determine the velocity profile in the outer region by considering the complete momentum equation (without the buoyancy term). The inner boundary condition for this outer region would be taken as the velocity at the edge of the inner layer. Since the heat transfer and skin friction results are not affected by the resulting "tail" of the velocity profile, it was not considered in the present analysis.

A comparison of theoretical and experimental temperature profiles for $n < 1$ in glycerine is presented in figure 4.2. Near the fin surface where temperature gradients are highest the scatter is small and the experimental points are consistently below the theoretical curve. Most of this effect can be attributed to conduction losses caused by the blunt point of the probe

* $\tilde{V} \cdot \nabla \theta$.

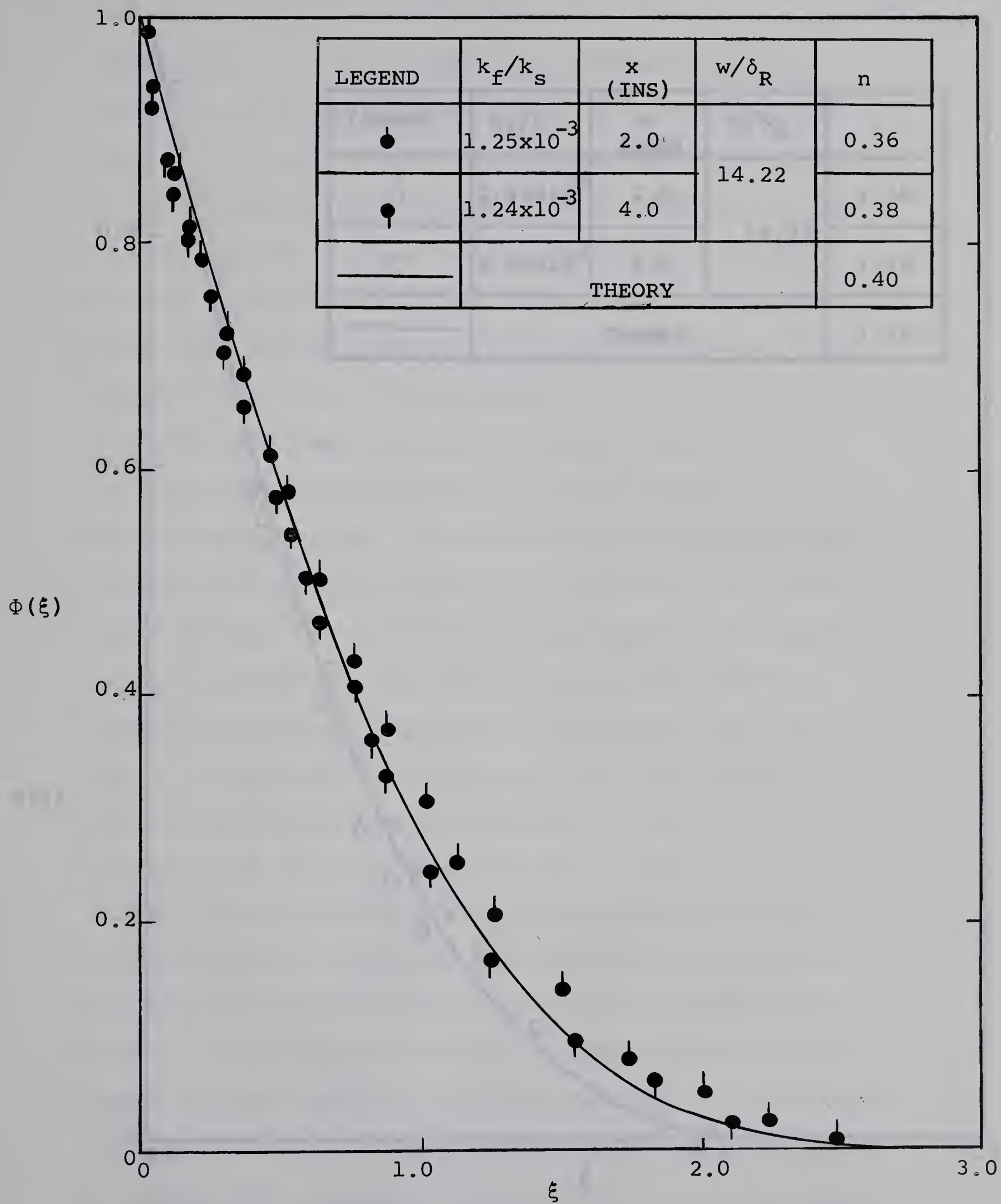


FIG. 4.2 Comparison of Temperature Profile (Glycerine)

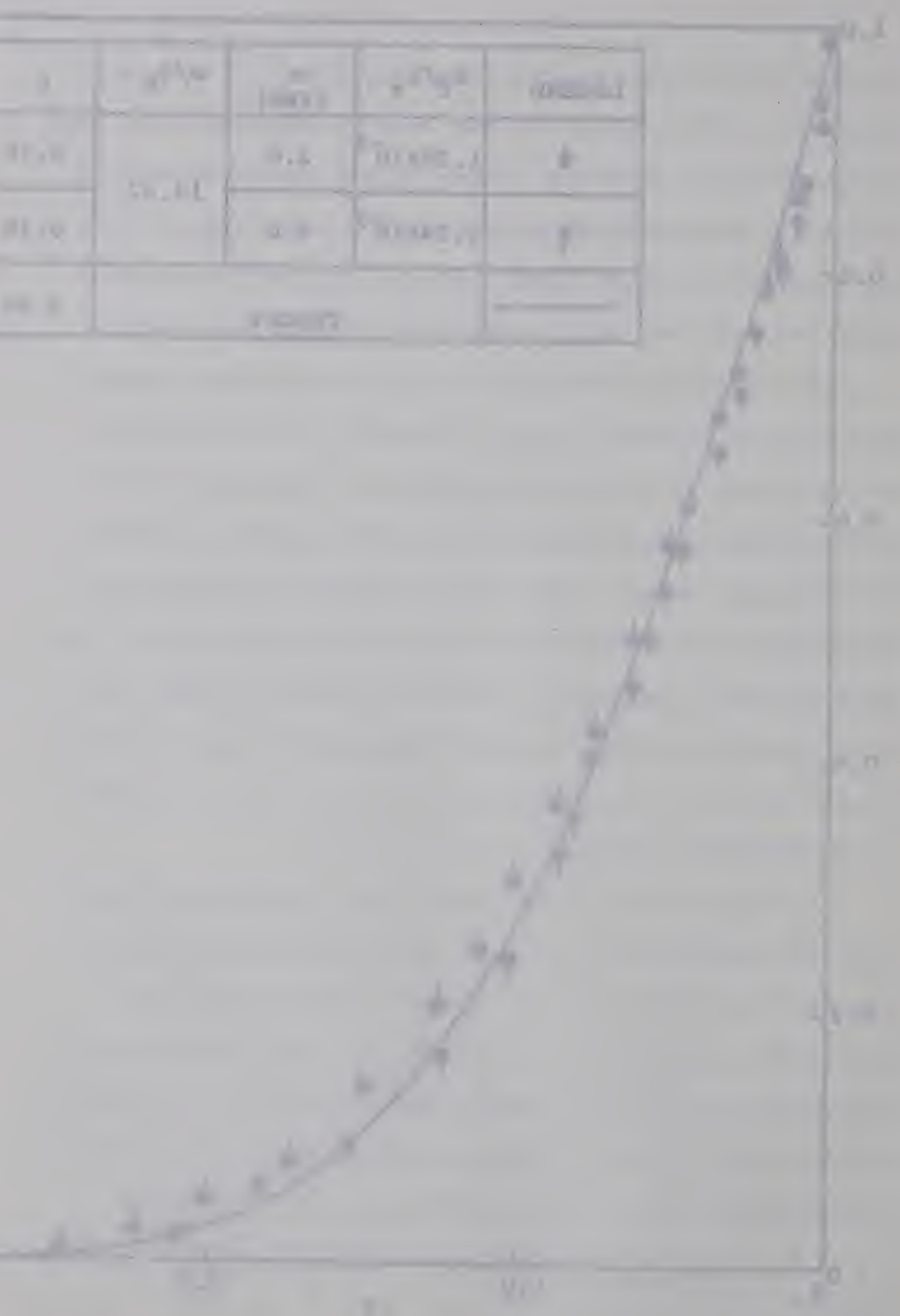


Figure 1: (a) (left) and (b) (right) relationship between the number of nodes (N) and the number of edges (E) for a sparse graph.

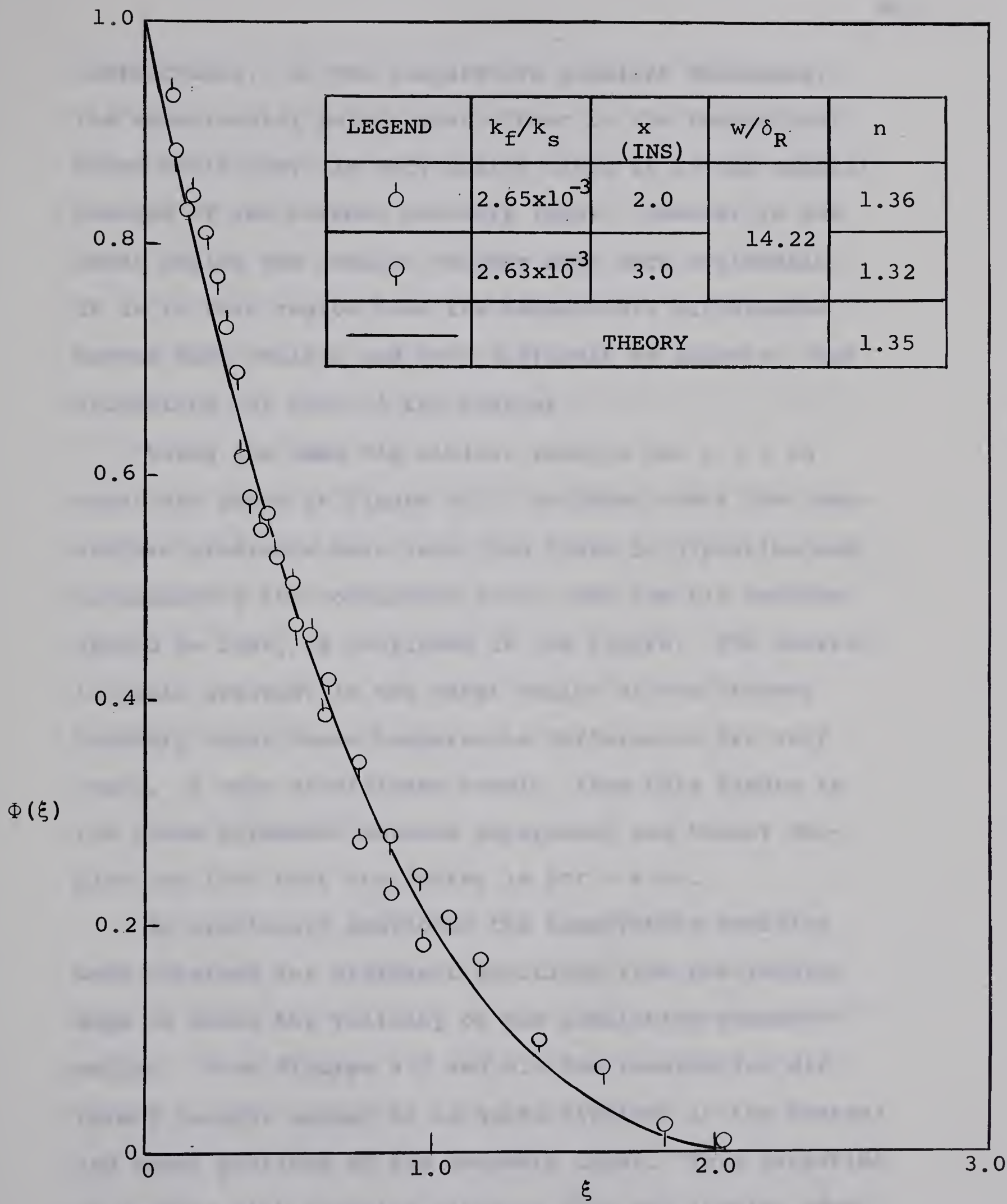


FIG. 4.3 Comparison of Temperature Profile (Water)

thermocouple. As the temperature gradient decreases, the experimental points move closer to the theoretical curve until they lie very nearly along it in the central portion of the thermal boundary layer. However in the outer region the scatter becomes much more noticeable. It is in this region that the temperature differences become much smaller and more difficult to measure, thus accounting for most of the scatter.

Using the same fin similar results for $n > 1$ in water are shown in figure 4.3. In these tests the temperature gradients were less than those in glycerine and consequently the conduction error near the fin surface should be less, as confirmed in the figure. The scatter is again greatest in the outer region of the thermal boundary layer where temperature differences are very small. A very significant result from this figure is the close agreement between experiment and theory despite the fact that the latter is for $\sigma = \infty$.

As previously mentioned the temperature profiles were obtained for different positions from the leading edge to check the validity of the similarity transformation. From figures 4.2 and 4.3 the results for different heights appear to be quite distinct in the central and outer portions of the boundary layer. This variation of results with changing distance from the leading edge,

if genuine, implies that the similarity variable ξ is incorrect. However as seen from the figures, this effect does not appear to be genuine because the points nearer the leading edge form the upper curve in glycerine and the lower curve in water. This reversal of results is not likely to be caused by changes in the Prandtl number. It is therefore concluded that the separation is mainly due to scatter caused by errors in measuring the small temperature differences.

Since the scatter of experimental results is nowhere large, figures 4.2 and 4.3 together reveal the overall effect of n on the temperature profiles. As predicted from the theory, an increase in n from about 0.4 in figure 4.2 to about 1.35 in figure 4.3 results in a steepening of the profile.

4.4 FIN EFFECTIVENESS

Utilizing the definition of fin effectiveness ϵ given in Chapter II resulted in figure 2.4, giving the relationship between ϵ and χ . By definition, the effectiveness may be greater or less than unity depending on whether the average heat flux is greater or less than the root heat flux. From equation (20) the surface heat flux, $h\theta_0$, varies as $\propto \frac{5n - 1}{4}$. Thus when $0 \leq n < \frac{1}{5}$ the

heat flux decreases monotonically from the leading edge so that $\epsilon > 1$. For the case of $n = \frac{1}{5}$ the surface heat flux becomes uniform and $\epsilon = 1$. Lastly, when $n > \frac{1}{5}$ the heat flux increases monotonically from the leading edge and consequently $\epsilon < 1$.

The results for $\sigma = 1$ and ∞ are effectively the same and thus imply that they will be accurate for all non-metallic liquids, if not all liquids. It is revealed from figure 2.4 that a change in effectiveness is more dependent on a change in χ than a separate change in σ (with χ fixed). This indicates that the effect of σ is largely contained in χ . This fact is further demonstrated by considering the results of the following tables A and B.

σ	$n = \frac{1}{5}$	
	γ	χ
∞	0.802	0.353
1	0.773	0.365
0	(0.920)	(0.308)

TABLE A

σ	χ	n	ϵ
∞	0.353	0.20	1.0
1	0.365	0.206	0.992
0	0.308	0.179	1.027

TABLE B

Although results are not available for $\gamma(n,0)$, other than $\gamma(0,0) = 0.849$, it is reasonable to expect that the shape of the γ versus n curve for $\sigma = 0$ will approximately

follow those for $\sigma = 1$ and ∞ , at least for small n . It is on this basis that a value $\gamma(\frac{1}{5}, 0) = 0.920$ was chosen. The γ were then used to determine the corresponding values of χ from equation (24), as shown in table A. The independent effect of σ is seen to be relatively small as there is a difference of only 12.5% between the values of χ for $\sigma = 0$ and $\sigma = \infty$.

However, as would occur in most practical cases, a value of χ would be known and it would be desired to evaluate the corresponding fin effectiveness ϵ . Table B considers the values of χ from table A, for which the actual values of n and ϵ are 0.2 and 1.0 respectively and from these are found corresponding values of n and ϵ by using the $\sigma = \infty$ results. The values of ϵ obtained in this manner demonstrate that the independent effect of σ on the fin effectiveness is very small. Thus the results shown in tables A and B, though not necessarily conclusive for all n , tend to reinforce the conclusion that a Prandtl number effect, other than that in χ , is sufficiently small to allow the use of the present heat transfer results for all Prandtl numbers.

4.5 BOUNDARY LAYER SHAPES

Photographs obtained in the Schlieren apparatus for the cases of $n < 0.2$ and $n > 1$ are shown in figures 4.4

and 4.5 respectively. The purpose of these was to verify the shape of the boundary layer and heat flux curve for differing values of n .

As mentioned in the previous section, the heat flux decreases monotonically from the leading edge when $0 \leq n < \frac{1}{5}$ and increases monotonically when $n > \frac{1}{5}$. These two facts are observed in figures 4.4 and 4.5 respectively.

An interesting feature of boundary layer growth is revealed by examination of the similarity variable ξ . The boundary layer thickness is found to vary as $x^{\frac{1-n}{4}}$ so that when $n < 1$ the thickness increases monotonically with height and decreases monotonically when $n > 1$. Of course, with $n = 0$ the familiar isothermal case occurs in which the thickness varies as $x^{1/4}$. When $n = 1$ the thickness is independent of height and therefore the boundary layer must be parallel to the surface. Visual confirmation of the effect of n on the boundary layer growth is obtained from the Schlieren photographs in figures 4.4 and 4.5.

Fin



FIG. 4.4 Schlieren Photograph ($n < 0.2$)



FIG. 4.5 Schlieren Photograph ($n > 1$)

CHAPTER V

CONCLUSIONS AND RECOMMENDATIONS

5.1 CONCLUSIONS

This thesis has described a theoretical and experimental investigation of the combined conduction-convection problem of heat transfer through and from a tapered, downward-projecting fin immersed in a quiescent, isothermal fluid. The theoretical analysis has demonstrated that a combined problem of this type may be solved "exactly" if certain simplifications are made in the individual conduction and convection problems. A power law solution for surface temperature was revealed after solving the convection problem separately and then applying the condition of continuity of temperature and heat flux at the common interface.

The overall heat transfer problem was found to be governed by a single non-dimensional group χ , which consists of a slenderness ratio, conductivity ratio and a variable Prandtl-Grashof number. The results were thus found to be dependent only on the overall geometry as opposed to the exact fin profile. The separate effect of Prandtl number on the results was found to be virtually negligible. In fact the temperature index and fin effectiveness were much more sensitive to changes in

root temperature, fin material and overall geometry than a separate change in the surrounding fluid. This separate independence of Prandtl number applies over the range $1 \leq \sigma \leq \infty$, if not the entire range.

The majority of the theoretical predictions were well borne out by the experimental results obtained. A comparison of theoretical and experimental results for the n versus χ relationship revealed agreement to within 10% or better. The experimental results clearly verified the overall trend.

Comparison of experimental and theoretical temperature profiles for water and glycerine revealed good overall agreement despite the fact the theoretical profiles were for $\sigma = \infty$. Discrepancies, although never large, were greatest in the outer region of the thermal boundary layer where temperature differences were very small and thus difficult to measure. Since the temperature profiles were found to be independent of distance from the leading edge of the fin, the validity of the similarity variable ξ was revealed.

The results and hence the conclusions, are only valid for the case of a single vertical fin or banks of vertical fins in which there are negligible effects of one fin upon another. The results for relatively small slenderness ratios are only valid where the fin conductivity is

sufficiently greater than that of the surrounding fluid, as in the experiments reported here and in most practical applications.

5.2 RECOMMENDATIONS

The analysis and thus the results, are limited to the behavior of a single vertical fin. A logical extension would be to consider multi-fin systems which are more likely to occur in practice. In this case an additional parameter enters into the problem, namely, the pitch/height ratio; this gives an indication of the effect of mutual proximity.

The only orientation considered for the fin in this analysis was that in a vertical downward-projecting position. Other positions such as horizontal, upward-projecting or angles in between these, could be studied. Also since no results were obtained for fins having curvature, studies could be carried out to determine these effects which would probably be some function of the radius of curvature. A cooled fin for which the flow would be reversed, at least for the vertical position, is another possibility for further analysis.

The validity of assumptions made in the theoretical section was ascertained with the use of experimental

temperature indexes and profiles only. A study of the experimental velocity profile would further verify the results and may also indicate the effect of neglecting the inertia terms for liquids whose Prandtl number is small. However, as in most free convection problems the velocities are small and very difficult to measure directly. One feasible method would likely be the use of the fibre anemometer. Dye streaks in glycerine and suspended particles in water will give indications of bulk fluid velocities.

The experimental results revealing the effects of slenderness ratio on the problem were all obtained for the case of a very high ratio of fin to fluid conductivity. Further tests with much smaller ratios should be performed to determine the possible effects of lateral temperature gradients in the fin.

Further investigations could be performed to determine whether or not the effect of Prandtl number is sufficiently contained in the variable Prandtl-Grashof number. A series of tests could therefore be performed in air and liquid metals to give an indication as to whether or not the predictions discussed in chapter IV are valid.

REFERENCES

1. SCHNEIDER, P.J., "Conduction Heat Transfer," Addison-Wesley Publishing Co., (1955).
2. SPARROW, E.M. and GREGG, J.L., "Laminar Free Convection From a Vertical Plate With Uniform Surface Heat Flux," Trans. ASME, Vol. 78, 1956, pp. 435-440.
3. SPARROW, E.M. and GREGG, J.L., "Similar Solutions for Free Convection from a Nonisothermal Vertical Plate," Trans. ASME, 1957, pp. 379-386.
4. WELLING, J.R. and WOOLDRIDGE, C.B., "Free Convection Heat Transfer Coefficients from Rectangular Vertical Fins," Trans. ASME, Series C, Vol. 87, 1965, pp. 439-444.
5. STARNER, K.E. and McMANUS, H.N. JR., "An Experimental Investigation of Free-Convection Heat Transfer from Rectangular Fin Array," Trans. ASME, Series C, Vol. 85, 1963, p. 273.
6. HSU, S.T., HSIEH, C. and VATSARAJ, B.C., "An Extended Surface with Finned Pins Under Free Convection Cooling," ASME Publication No. 65-HT-55.
7. KNUDSEN, J.G. and PAN, R.B., "Natural Convection Heat Transfer from Transverse Finned Tubes," Chemical Engineering Progress Symposium Series, No. 57, Vol. 61, 1965, p. 44.
8. SPARROW, E.M. and GREGG, J.L., "The Variable Fluid - Property Problem in Free Convection," Trans. ASME, Vol. 80, 1958, p. 879.
9. YANG, K.T., "Possible Similarity Solutions for Laminar Free Convection on Vertical Plates and Cylinders," Trans. ASME, Series E, Vol. 82, 1960, pp. 230-236.
10. LOCK, G.S.H., "Steady Laminar Free Convection from Inclined Arbitrarily Shaped Plane Surfaces," Int. Jour. Heat and Mass Transfer, Vol. 7, 1964, pp. 669-673.
11. LEFEVRE, E.J., "Laminar Free Convection from a Vertical Plane Surface," Heat Division Paper 113, Mech. Eng. Res. Lab., Dept. Sci. and Ind. Res., Glasgow, 1956.

12. MEKSYN, D., "New Methods in Laminar Boundary Layer Theory," Pergamon, London, 1961.
13. BRINDLEY, J., "An Approximation Technique for Natural Convection in a Boundary Layer," Int. Jour. Heat and Mass Transfer, Vol. 6, 1963, p. 1035.
14. KREITH, K., "Principles of Heat Transfer", sixth printing (1962), International Textbook Company, Scranton.
15. OSTRACH, S., "An Analysis of Laminar Free-Convection Flow and Heat Transfer About a Flat Plate Parallel to the Direction of the Generating Body Force," NACA TR 1111, 1953.

APPENDIX A

FORTRAN IV PROGRAM FOR EIGENVALUE SOLUTION

The computer program used to compute the values of α and γ versus n follows this introduction. Assuming initial numerical values for $\alpha(\equiv A)$ and $\gamma(\equiv B)$ the program sets $n(\equiv H)$ to zero and calculates the values of the coefficients $a_r(\equiv Ar)$, $b_r(\equiv Br 1)$, $b_r'(\equiv Br 2)$, $c_r(\equiv Cr)$, $d_s(\equiv Ds 1)$ and $g_s(\equiv Ds 2)$. From the d_s and the $\Gamma\left(\frac{s+1}{3}\right)(\equiv Gs)$ are formed the products, $d_s\Gamma\left(\frac{s+1}{3}\right)(\equiv Rs 1)$, which are then transferred to the subroutine (EULER) to check the convergence and apply Euler's transformation if necessary. This same procedure is carried out for the products

$$g_s \left(\frac{s+1}{3}\right) (\equiv Rs 2).$$

The series $\sum d_s \Gamma\left(\frac{s+1}{3}\right) (\equiv S(I))$ and $\sum g_s \Gamma\left(\frac{s+1}{3}\right) (\equiv R(J))$ are both summed and checked against their known and specified correct value. If they are incorrect either α or γ is incremented and the coefficients and series are then recalculated. This iteration procedure is repeated until both $S(I)$ and $R(J)$ assume acceptable values. Once the latter are obtained $n(\equiv H)$ is incremented a given amount and the whole procedure is repeated, using as initial values of α and γ the values obtained for the previous n .


```

$IBFTC EIGENS NOLIST, NODECK
DIMENSION S(3000), R(3000)
A=.82450000
B=.71000000
G0=2.6789385347
G1=1.3541179394
G2=1.0000000000
G3=0.8929795116
G4=0.9027452929
G5=1.0000000000
G6=1.1906393488
60
C GN ARE THE GAMMA FUNCTIONS
DO 11 K=0,50
P=K
H=P/10.
I=1
J=1
N=0
M=0
G=1.0
T=1.0
C=0.0
L=0
F=0.0
D=0.0
SS=0.0
RR=0.0
WRITE(6,50)H
20 A2=A
A3=-1.0
A4=B
A5=0.0
A6=-4.*H*A
A7=4.*H+(7.*H-3.)*B*A
A8=(3.-15.*H)*B
C0=(H+3.)*A2/6.
C1=(H+3.)*A3/24.
C2=(H+3.)*A4/120.
C3=0.0
C4=(H+3.)*A6/5040.
C5=(H+3.)*A7/40320.
C6=(H+3.)*A8/362880.
B01=B
B11=0.0
B21=-4.*H*A
B31=4.*H*(1.+2.*A*B)
B41=-16.*H*B
B51=16.*H*(B*B-5.*H*A*A-3.*A*A)
B61=(316.*H*H*A+220.*H*H*A*A*B+180.*H*A*A*B+180.*H*A)
B02=-1.
B12=B
B22=0.0
B32=-A*(5.*H+3.)
B42=(5.*H+3.+A*B*(11.*H+9.))
B52=-B*(21.*H+15.)
B62=(21.*H*B*B+15.*B*B-130.*H*H*A*A-228.*H*A*A-90.*A*A)
D01=B01/(3.*C0**.3333333)
D11=-2.*B01*C1/(9.*C0**1.66666667)
D21=(B01*(C1/C0)**2-B01*C2/C0+B21/2.)/(3.*C0)
D31=(B31/6.-2.*B21*C1/(3.*C0)+B01*(28.*C1*C2/(9.*C0**2))-140.*((C1/

```



```

1C0)**3)/81.))/((3.*C0**1.33333333)
D41=(B41/24.-5.*B31*C1/(18.*C0)+B21*(-5.*C2/(3.*C0)+20.*((C1/C0)**
12)/9.)/2.+B01*(-5.*C4/(3.*C0)+20.*((C2/C0)**2)/9.-220.*((C1)**2)*C2
2/(C0**3))/27.+770.*((C1/C0)**4)/243.))/((3.*C0**1.66666667)
D51=(B51/120.-B41*C1/(12.*C0)+B31*(-2.*C2/C0+3.*((C1/C0)**2))/6.+B
121*(6.*C1*C2/(C0**2)-4.*((C1/C0)**3)/2.+B01*(-2.*C5/C0+6.*C1*C4/(C0
2**2)-12.*C1*(C2**2)/(C0**3)+20.*C2*(C1**3)/(C0**4)-6.*((C1/C0)**5))
3/(3.*C0**2)
D61=(B61/720.-7.*B51*C1/(360.*C0)+B41*(-7.*C2/(3.*C0)+35.*((C1/C0)
1**2)/9.)/24.+B31*(70.*C1*C2/(9.*C0**2)-455.*((C1/C0)**3)/81.)/6.+B
221*(-7.*C4/(3.*C0)+35.*((C2/C0)**2)/9.-455.*C2*(C1**2)/(27.*C0**3)
3+1820.*((C1/C0)**4)/243.)/2.+B01*(-7.*C6/(3.*C0)+70.*((C1*C5+C2*C4)
4/(9.*C0**2)-455.*((3.*C4*(C1**2)+(C2**3)))/(81.*C0**3)+5460.*((C1**2)
5*(C2**2)/(81.*C0**4)-34580.*C2*(C1**4)/(729.*C0**5)+76076.*((C1/C0
6)**6)/6561.))/((3.*C0**2.33333333)
D02=B02/(3.*C0**.33333333)
D12=(B12-2.*B02*C1/(3.*C0))/((3.*C0**.66666666)
D22=(B02*((C1/C0)**2-C2/C0)-B12*C1/C0)/(3.*C0)
D32=(B32/6.+B12*(-4.*C2/(3.*C0)+14.*((C1/C0)**2)/9.))+B02*(28.*C1*C
12/(9.*C0**2)-140.*((C1/C0)**3)/81.))/((3.*C0**1.33333333)
D42=(B42/24.-5.*B32*C1/(18.*C0)+B12*(40.*C1*C2/(9.*C0**2)-220.*((C
21/C0)**3)/81.))+B02*(-5.*C4/(3.*C0)+20.*((C2/C0)**2)/9.-220.*C2*(C1
3**2)/(27.*C0**3)+770.*((C1/C0)**4)/243.))/((3.*C0**1.66666667)
D52=(B52/120.-B42*C1/(12.*C0)+B32*(-2.*C2/C0+3.*((C1/C0)**2))/6.+B
112*(-2.*C4/C0+3.*((C2/C0)**2)-12.*C2*(C1**2)/(C0**3)+5.*((C1/C0)**
24))+B02*(-2.*C5/C0+6.*C1*C4/(C0**2)-12.*C1*(C2**2)/(C0**3)+20.*C2*
3*(C1**3)/(C0**4)-6.*((C1/C0)**5)))/((3.*C0**2)
D62=(B62/720.-7.*B52*C1/(360.*C0)+B42*(-7.*C2/(3.*C0)+35.*((C1/C0)
1**2)/9.)/24.+B32*(70.*C1*C2/(9.*C0**2)-455.*((C1/C0)**3)/81.)/6.+B
212*(-7.*C5/(3.*C0)+70.*C1*C4/(9.*C0**2)-455.*C1*(C2**2)/(27.*C0**3
3)+7280.*C2*(C1**3)/(243.*C0**4)-6916.*((C1/C0)**5)/729.))+B02*(-7.*
4C6/(3.*C0)+70.*((C1*C5+C2*C4)/(9.*C0**2)-455.*((3.*C4*(C1**2)+(C2**3
5))/(81.*C0**3)+5460.*((C1**2)*(C2**2)/(81.*C0**4)-34580.*C2*(C1**4)
6/(729.*C0**5)+76076.*((C1/C0)**6)/6561.))/((3.*C0**2.33333333)
R01=D01*G0
R11=D11*G1
R21=D21*G2
R31=D31*G3
R41=D41*G4
R51=D51*G5
R61=D61*G6
T0=R01
T1=R11
T2=R21
T3=R31
T4=R41
T5=R51
T6=R61
CALL EULER(T0,T1,T2,T3,T4,T5,T6)
R01=T0
R11=T1
R21=T2
R31=T3
R41=T4
R51=T5
R61=T6
R02=D02*G0
R12=D12*G1
R22=D22*G2
R32=D32*G3

```



```

R42=D42*G4
R52=D52*G5
R62=D62*G6
T0=R02
T1=R12
T2=R22
T3=R32
T4=R42
T5=R52
T6=R62
CALL EULER(T0,T1,T2,T3,T4,T5,T6)
R02=T0
R12=T1
R22=T2
R32=T3
R42=T4
R52=T5
R62=T6
S(I)=R01+R11+R21+R31+R41+R51+R61
R(J)=R02+R12+R22+R32+R42+R52+R62
IF(D.GT.0.0)GO TO 40
IF(M.GT.0) GO TO 35
IF(N.GT.0) GO TO 30
U=0.2*(ABS(S(I)-1.0))
A=A+G*U*A
N=N+1
I=I+1
J=J+1
GO TO 20
30 Z=ABS(S(I)-1.0)
W=ABS(S(I-1)-1.0)
IF(Z.GT.W)G=-G
IF(Z.LE.0.001) GO TO 46
45 U=0.2*(ABS(S(I)-1.0))
A=A+2.*G*U*A
M=M+1
J=J+1
I=I+1
N=0
GO TO 20
35 C=C+1.0
IF(L.GT.0)GO TO 31
V=0.2*(ABS((R(J)+A)/A))
B=B+T*V*B
I=I+1
J=J+1
L=L+1
GO TO 20
31 Q=ABS(R(J)+A)
X=ABS(R(J-1)+A)
IF(Q.GT.X)T=-T
IF(Q.LE.0.001) GO TO 72
73 V=0.2*(ABS((R(J)+A)/A))
B=B+2.*T*V*B
I=I+1
J=J+1
L=0
D=D+1.0
GO TO 20
40 M=0

```



```

IF(RR.GT.0.0) GO TO 41
IF(SS.GT.0.0) GO TO 42
U=0.2*(ABS((R(J)+A)/A))
A=A+G*U*A
SS=SS+1.0
I=I+1
J=J+1
GO TO 20
42 Q=ABS(R(J)+A)
X=ABS(R(J-1)+A)
IF(Q.GT.X)G==G
IF(Q.LE.0.001) GO TO 70
71 U=0.2*(ABS((R(J)+A)/A))
A=A+2.*G*U*A
RR=RR+1.0
I=I+1
J=J+1
GO TO 20
41 SS=0.0
IF(E.GT.0.0) GO TO 43
V=0.2*(ABS(S(I)-1.0))
B=B+T*V*B
I=I+1
J=J+1
E=E+1.0
GO TO 20
43 Z=ABS(S(I)-1.0)
W=ABS(S(I-1)-1.0)
IF(Z.GT.W)T==T
IF(Z.LE.0.001) GO TO 74
75 V=0.2*(ABS(S(I)-1.0))
B=B+2.*T*V*B
I=I+1
J=J+1
F=0.0
RR=0.0
D=0.0
GO TO 20
46 Q=ABS(R(J)+A)
IF(Q.LE.0.001) GO TO 10
GO TO 45
72 Z=ABS(S(I)-1.0)
IF(Z.LE.0.001) GO TO 10
GO TO 73
70 Z=ABS(S(I)-1.0)
IF(Z.LE.0.001) GO TO 10
GO TO 71
74 Q=ABS(R(J)+A)
IF(Q.LE.0.001) GO TO 10
GO TO 75
10 WRITE(6,52)R01,R11,R21,R31,R41,R51,R61
      WRITE(6,52)R02,R12,R22,R32,R42,R52,R62
      WRITE(6,51)A,B,S(I),R(J)
11 CONTINUE
STOP
50 FORMAT(2X,23HTEMPERATURE EXPONENT = ,F8.4/)
51 FORMAT(2X,9H ALPHA = ,F12.8,9H GAMMA = ,F12.8,8H SUM1 = F12.8,8H S
      1UM2 = ,F12.8/)
52 FORMAT(5X,6F12.6,F14.8)
END

```


\$IBFTC EULER NOLIST, NODECK

SUBROUTINE EULER(T0,T1,T2,T3,T4,T5,T6)

DIMENSION R0(250),R1(250),R2(250),R3(250),R4(250),R5(250),R6(250)

AB=1.

MN=1

R0(MN)=T0

R1(MN)=T1

R2(MN)=T2

R3(MN)=T3

R4(MN)=T4

R5(MN)=T5

R6(MN)=T6

IF(ABS(R1(MN)).GE.ABS(R0(MN))) GO TO 500

IF(ABS(R2(MN)).GE.ABS(R1(MN))) GO TO 500

IF(ABS(R3(MN)).GE.ABS(R2(MN))) GO TO 500

IF(ABS(R4(MN)).GE.ABS(R3(MN))) GO TO 500

IF(ABS(R5(MN)).GE.ABS(R4(MN))) GO TO 500

IF(ABS(R6(MN)).GE.ABS(R5(MN))) GO TO 500

NM=MN

GO TO 501

500 MN=MN+1

NM=50

JK=50

R6(NM)=.500

600 F0=R0(MN-1)

F1=R0(MN-1)+R1(MN-1)

F2=F1+R1(MN-1)+R2(MN-1)

F3=F2+R1(MN-1)+2.*R2(MN-1)+R3(MN-1)

F4=F3+R1(MN-1)+3.*R2(MN-1)+3.*R3(MN-1)+R4(MN-1)

F5=F4+R1(MN-1)+4.*R2(MN-1)+6.*R3(MN-1)+4.*R4(MN-1)+R5(MN-1)

F6=F5+R1(MN-1)+5.*R2(MN-1)+10.*R3(MN-1)+10.*R4(MN-1)+5.*R5(MN-1)+R6(MN-1)

R0(MN)=F0/2.

R1(MN)=F1/4.

R2(MN)=F2/8.

R3(MN)=F3/16.

R4(MN)=F4/32.

R5(MN)=F5/64.

R6(MN)=F6/128.

IF(ABS(R1(MN)).GT.ABS(R0(MN))) GO TO 401

IF(ABS(R2(MN)).GT.ABS(R1(MN))) GO TO 401

IF(ABS(R3(MN)).GE.ABS(R2(MN))) GO TO 401

IF(ABS(R4(MN)).GE.ABS(R3(MN))) GO TO 401

IF(ABS(R5(MN)).GE.ABS(R4(MN))) GO TO 401

IF(ABS(R6(MN)).GE.ABS(R5(MN))) GO TO 401

IF(ABS(R6(MN)).LT.ABS(R6(NM))) NM=MN

401 CONTINUE

MN=MN+1

KK=MN-2

F1=R1(KK)

F2=R1(KK)+R2(KK)

F3=F2+R2(KK)+R3(KK)

F4=F3+R2(KK)+2.*R3(KK)+R4(KK)

F5=F4+R2(KK)+3.*R3(KK)+3.*R4(KK)+R5(KK)

F6=F5+R2(KK)+4.*R3(KK)+6.*R4(KK)+4.*R5(KK)+R6(KK)

R0(MN)=R0(KK)

R1(MN)=F1/2.

R2(MN)=F2/4.

R3(MN)=F3/8.

R4(MN)=F4/16.


```

R5(MN)=F5/32.
R6(MN)=F6/64.
IF(ABS(R1(MN)).GT.ABS(R0(MN))) GO TO 403
IF(ABS(R2(MN)).GT.ABS(R1(MN))) GO TO 403
IF(ABS(R3(MN)).GE.ABS(R2(MN))) GO TO 403
IF(ABS(R4(MN)).GE.ABS(R3(MN))) GO TO 403
IF(ABS(R5(MN)).GE.ABS(R4(MN))) GO TO 403
IF(ABS(R6(MN)).GE.ABS(R5(MN))) GO TO 403
IF(ABS(R6(MN)).LT.ABS(R6(NM))) NM=MN

403 CONTINUE
MN=MN+1
KK=MN-3
F2=R2(KK)
F3=R2(KK)+R3(KK)
F4=F3+R3(KK)+R4(KK)
F5=F4+R3(KK)+2.*R4(KK)+R5(KK)
F6=F5+R3(KK)+3.*R4(KK)+3.*R5(KK)+R6(KK)
R0(MN)=R0(KK)
R1(MN)=R1(KK)
R2(MN)=F2/2.
R3(MN)=F3/4.
R4(MN)=F4/8.
R5(MN)=F5/16.
R6(MN)=F6/32.
IF(ABS(R1(MN)).GE.ABS(R0(MN))) GO TO 409
IF(ABS(R2(MN)).GF.ABS(R1(MN))) GO TO 409
IF(ABS(R3(MN)).GE.ABS(R2(MN))) GO TO 409
IF(ABS(R4(MN)).GF.ABS(R3(MN))) GO TO 409
IF(ABS(R5(MN)).GE.ABS(R4(MN))) GO TO 409
IF(ABS(R6(MN)).GF.ABS(R5(MN))) GO TO 409
IF(ABS(R6(MN)).LT.ABS(R6(NM))) NM=MN

409 CONTINUE
MN=MN+1
F3=R3(KK)
F4=R3(KK)+R4(KK)
F5=F4+R4(KK)+R5(KK)
F6=F5+R4(KK)+2.*R5(KK)+R6(KK)
R0(MN)=R0(KK)
R1(MN)=R1(KK)
R2(MN)=R2(KK)
R3(MN)=F3/2.
R4(MN)=F4/4.
R5(MN)=F5/8.
R6(MN)=F6/16.
IF(ABS(R1(MN)).GE.ABS(R0(MN))) GO TO 405
IF(ABS(R2(MN)).GE.ABS(R1(MN))) GO TO 405
IF(ABS(R3(MN)).GE.ABS(R2(MN))) GO TO 405
IF(ABS(R4(MN)).GF.ABS(R3(MN))) GO TO 405
IF(ABS(R5(MN)).GE.ABS(R4(MN))) GO TO 405
IF(ABS(R6(MN)).GE.ABS(R5(MN))) GO TO 405
IF(ABS(R6(MN)).LT.ABS(R6(NM))) NM=MN

405 CONTINUE
MN=MN+1
F4=R4(KK)
F5=R4(KK)+R5(KK)
F6=F5+R5(KK)+R6(KK)
R0(MN)=R0(KK)
R1(MN)=R1(KK)
R2(MN)=R2(KK)
R3(MN)=R3(KK)

```

(२०१२९ + १९२) २८५ * ८५ + (१११६८ + १२३ - १२५)

$$B_1(M) = \{M\} \cup \{M \otimes N \mid N \in B_1(M)\}$$

- $\Delta \setminus \mathcal{S}^2 = (NM) \setminus \mathcal{S}^2$
- $\mathcal{R} \setminus \Delta^2 = (NM) \setminus \mathcal{R}^2$

1998 07 26 (((NM) 58) 235-33- (((NM) 58) 238A) 13

198 07 26 ((LVM) 99) 2 10.72 0.198 (LVM) 198 198 07 26 ((LVM) 100) 2 10.72 0.198 (LVM) 198

CONTINUOUS
F+MM=MM
CROSSING OF

$$E\Delta = E\Delta (A\Delta) + E\Delta (A\Delta + B\Delta) + E\Delta (B\Delta + C\Delta) + E\Delta (C\Delta + A\Delta)$$

$$LA = 32 + 8\Delta(144) + 5 \cdot 8\Delta(172) + 10\Delta(196)$$

$$B_2(\omega) = \Gamma(\omega) - \Gamma(-\omega)$$

- ८१. $\overline{Z} = (1M) \overline{M}$
- ८२. $\overline{M} = (1M) \overline{M}$

• 128 (M) = 5 = 18. • 128 (M) = 29 • 128 (M) = 18. • 128 (M) = 18.

•T• ((4M1A6)29A)131
•T• ((4M1A6)29A)131

1. $(\text{N} + \text{O}) + (\text{N} + \text{O}) = \text{NO}_2$
2. $(\text{N} + \text{O}) + (\text{N} + \text{O}) = \text{NO}_2$

$$(M^*) \cap \mathcal{Q} = (M \cap \mathcal{Q})^*$$

```

R4(MN)=F4/2.
R5(MN)=F5/4.
R6(MN)=F6/8.
IF(ABS(R1(MN)).GE.ABS(R0(MN))) GO TO 407
IF(ABS(R2(MN)).GE.ABS(R1(MN))) GO TO 407
IF(ABS(R3(MN)).GE.ABS(R2(MN))) GO TO 407
IF(ABS(R4(MN)).GE.ABS(R3(MN))) GO TO 407
IF(ABS(R5(MN)).GE.ABS(R4(MN))) GO TO 407
IF(ABS(R6(MN)).GE.ABS(R5(MN))) GO TO 407
IF(ABS(R6(MN)).LT.ABS(R6(NM))) NM=MN

407 CONTINUE
MN=MN+1
F5=R5(KK)
F6=R5(KK)+R6(KK)
R0(MN)=R0(KK)
R1(MN)=R1(KK)
R2(MN)=R2(KK)
R3(MN)=R3(KK)
R4(MN)=R4(KK)
R5(MN)=F5/2.
R6(MN)=F6/4.
IF(ABS(R1(MN)).GE.ABS(R0(MN))) GO TO 400
IF(ABS(R2(MN)).GE.ABS(R1(MN))) GO TO 400
IF(ABS(R3(MN)).GE.ABS(R2(MN))) GO TO 400
IF(ABS(R4(MN)).GE.ABS(R3(MN))) GO TO 400
IF(ABS(R5(MN)).GE.ABS(R4(MN))) GO TO 400
IF(ABS(R6(MN)).GE.ABS(R5(MN))) GO TO 400
IF(ABS(R6(MN)).LT.ABS(R6(NM))) NM=MN

400 CONTINUE
IF(NM.NE.JK) GO TO 501
MN=KK+1
GO TO 500
501 T0=R0(NM)
T1=R1(NM)
T2=R2(NM)
T3=R3(NM)
T4=R4(NM)
T5=R5(NM)
T6=R6(NM)
RETURN
END

$ENTRY      EIGENS

```


APPENDIX B

FORTRAN IV PROGRAM FOR VELOCITY AND TEMPERATURE PROFILES

Once the eigenvalues α and γ have been obtained it is a simple matter to calculate the velocity and temperature profiles by forward integration. The computer program used for this purpose follows this brief introduction. The values of the eigenvalues $\alpha (\equiv C(K))$ and $\gamma (\equiv D(K))$ are first read in for each value of $n (\equiv K)$. Then utilizing a fourth degree polynomial the program calculates corresponding values for the following, versus $\xi (\equiv XI)$:

$$F(\xi) \equiv F_0(I)$$

$$F'(\xi) \equiv F_1(I)$$

$$F''(\xi) \equiv F_2(I)$$

$$F'''(\xi) \equiv F_3(I)$$

$$F^{IV}(\xi) \equiv F_4(I)$$

$$F^V(\xi) \equiv F_5(I)$$

\$IBFTC VELTEM NOLIST, NODECK

```

DIMENSION C(300),D(300),F0(300),F1(300),F2(300),F3(300),F4(300),F5
1(300)
N=31
E=0.05
READ(5,51)(C(K),D(K),K=1,N)
DO 10 K=1,N
P=K
H=(P-1.)/10.
WRITE(6,50)H
WRITE(6,52)
A=C(K)
B=D(K)
20 A2=A
A3=-1.0
A4=B
A6=-4.*H*A
A7=4.*H+(7.*H-3.)*B*A
A8=(3.-15.*H)*B
A9=(18.-10.*H)*(4.*H*A*A)+(15.*H-3.)*B*B
A10=176.*H*H*A-240.*H*A+70.*H*H*A*A*B-240.*H*A*A*B+90.*A*A*B
A11=1446.*H*A*B-795.*H*H*A*B-315.*A*B-176.*H*H+240.*H
A12=-280.*(H**3)*(A**3)+3024.*H*H*(A**3)+1029.*H*H*A*B*B-2118.*H*A
1*B*B-2166.*H*B+1323.*H*H*A-4536.*H*(A**3)+513.*A*B*B+315.*B
DO 5 I=1,4
TT=I
XI=(TT-1.)/20.
F0(I)=A2*(XI**2)/2.+A3*(XI**3)/6.+A4*(XI**4)/24.+A6*(XI**6)/720.+A
17*(XI**7)/5040.+A8*(XI**8)/40320.
F1(I)=A2*XI+A3*(XI**2)/2.+A4*(XI**3)/6.+A6*(XI**5)/120.+A7*(XI**6)
1/720.+A8*(XI**7)/5040.+A9*(XI**8)/40320.
F2(I)=A2+A3*XI+A4*(XI**2)/2.+A6*(XI**4)/24.+A7*(XI**5)/120.+A8*(XI
1**6)/720.+A9*(XI**7)/5040.+A10*(XI**8)/40320.
F3(I)=A3+A4*XI+A6*(XI**3)/6.+A7*(XI**4)/24.+A8*(XI**5)/120.+A9*(XI
1**6)/720.+A10*(XI**7)/5040.+A11*(XI**8)/40320.
F4(I)=A4+A6*(XI**2)/2.+A7*(XI**3)/6.+A8*(XI**4)/24.+A9*(XI**5)/120
1.+A10*(XI**6)/720.+A11*(XI**7)/5040.+A12*(XI**8)/40320.
F5(I)=4.*H*F3(I)*F1(I)-(H+3.)*F4(I)*F0(I)
5 WRITE(6,53)XI,F0(I),F1(I),F2(I),F3(I),F4(I),F5(I)
I=5
15 I1=I-1
I2=I-2
I3=I-3
I4=I-4
TT=I
XI=(TT-1.)/20.
F0(I)=F0(I1)+E*(F1(I1)+0.5*(F1(I1)-F1(I2))+5.*(F1(I1)-2.*F1(I2)+F1
1(I3)))/12.+3.*(F1(I1)-3.*F1(I2)+3.*F1(I3)-F1(I4))/8.
F1(I)=F1(I1)+E*(F2(I1)+0.5*(F2(I1)-F2(I2))+5.*(F2(I1)-2.*F2(I2)+F2
1(I3)))/12.+3.*(F2(I1)-3.*F2(I2)+3.*F2(I3)-F2(I4))/8.
F2(I)=F2(I1)+E*(F3(I1)+0.5*(F3(I1)-F3(I2))+5.*(F3(I1)-2.*F3(I2)+F3
1(I3)))/12.+3.*(F3(I1)-3.*F3(I2)+3.*F3(I3)-F3(I4))/8.
F3(I)=F3(I1)+E*(F4(I1)+0.5*(F4(I1)-F4(I2))+5.*(F4(I1)-2.*F4(I2)+F4
1(I3)))/12.+3.*(F4(I1)-3.*F4(I2)+3.*F4(I3)-F4(I4))/8.
F4(I)=F4(I1)+E*(F5(I1)+0.5*(F5(I1)-F5(I2))+5.*(F5(I1)-2.*F5(I2)+F5
1(I3)))/12.+3.*(F5(I1)-3.*F5(I2)+3.*F5(I3)-F5(I4))/8.
F5(I)=4.*H*F3(I)*F1(I)-(H+3.)*F4(I)*F0(I)
11 WRITE(6,53)XI,F0(I),F1(I),F2(I),F3(I),F4(I),F5(I)
IF(ABS(F3(I)).LT.0.01) GO TO 10
I=I+1

```



```
MN=1
GO TO 15
10  CONTINUE
STOP
50  FORMAT(2X,23HTEMPERATURE EXPONENT = ,F8.4/)
52  FORMAT(5X,2HXI,9X,2HF0,12X,2HF1,12X,2HF2,12X,2HF3,12X,2HF4,12X,2HF
15)
53  FORMAT(2X,F8.3,6F14.8)
51  FORMAT(8F10.6)
END
$ENTRY VELTEM
```

100	100
100	100
100	100
100	100
100	100

APPENDIX C

DATA REDUCTION

The typical procedure used in reducing the experimental data is illustrated by considering a test in glycerine for $w/\delta_R = 14.22$. Firstly, all thermocouple readings were converted to temperatures using the conversion chart for iron-constantan thermocouples. The surface temperatures, θ_0 , were then plotted versus (x/w) on log-log paper and the temperature index n was determined from the slope of this straight line. Since in most cases there was not a thermocouple located exactly at the root, θ_R was evaluated by extending the plot back to $x/w = 1$. For the example under consideration, $n = 0.363 \pm 9.8\%$ and $\theta_R = 12.35^\circ\text{F} \pm 1.2\%$.

In order to evaluate the theoretical n from figure 2.3 it was necessary to determine the numerical value of χ . For evaluating this, a bulk fluid temperature was required since several fluid properties were needed. The average surface temperature, $\theta_{0\text{avg}}$, was taken as

$$\frac{\int_0^w \theta_0 dx}{w} = \frac{\theta_R}{(n + 1)}, \text{ which gave } \theta_{0\text{avg}} = 9.06^\circ\text{F} \pm 11.0\%.$$

This along with $T_\infty = 67.27^\circ\text{F}$ resulted in a bulk fluid temperature of $T_{\text{BULK}} = 71.80^\circ\text{F} \pm 11.5\%$.

Properties were obtained from tables [14], giving

$\sigma = 11.65 \times 10^3 \pm 3.0\%$, $\frac{\beta q}{2} = 88 \pm 4.0\% \text{ l/}^{\circ}\text{F ft}^3$,
 $k_f = .165 \pm 0.5\% \text{ BTU/hr.ft.}^{\circ}\text{F}$ and $k_s = 132 \pm 2.0\% \text{ BTU/hr.ft.}^{\circ}\text{F}$.

Using these values,

$$\chi = \left(\frac{k_f}{k_s} \right) \left(\frac{w}{\delta_R} \right) \left[\frac{\beta q \theta_R w^3}{\kappa^2 (1+\sigma)} \right]^{1/4} = 0.700 \pm 6.0\%.$$

Considering the experimental temperature profile for a typical point in the boundary layer,

$$x = 2" \pm 0.05$$

$$y = 0.095" \pm 0.002$$

$$\theta(x, y) = 4.82^{\circ}\text{F} \pm 0.1$$

$$w = 6.938" \pm 0.002$$

$$\xi = \left[\frac{\beta q \theta_R}{4\kappa^2 w^n (1+\sigma)} \right]^{1/4} \frac{y}{x^{\frac{1-n}{4}}} = 0.467 \pm 6.1\%$$

$$\Phi(\xi) = \frac{\theta(x, y)}{\theta_R \left(\frac{x}{w} \right)^n} = 0.612 \pm 5.7\%$$

These percentage errors, though calculated for the central region of the thermal boundary layer in glycerine, are indicative of the magnitude of the errors for all tests performed.

APPENDIX D

AN ALTERNATIVE SOLUTION

During the course of attempting to solve the governing fifth order non-linear equation (9), several other numerical and analytical methods were tried. One of the numerical methods worth noting is a combination of numerical integration and iteration. The Fortran IV computer program used for this method will follow the outline of the procedure used.

The uncombined form of equation (9),

$$F''' + \Phi = 0 \quad (D1)$$

$$\Phi'' + (n+3) F\Phi' - 4n F'\Phi = 0 \quad (D2)$$

is the starting point. Formally solving (D2) as a linear non-homogeneous first order equation in Φ' results in

$$\Phi'(\xi) = e^{-\int_0^\xi (n+3)F d\xi} \int_0^\xi 4n F' \Phi e^{\int_0^\xi (n+3)F d\xi} d\xi - \int_0^\xi (n+3)F d\xi + \Phi'(0) e^{\int_0^\xi (n+3)F d\xi} \quad (D3)$$

Integrating (D3) once and using the boundary condition, $\Phi'(0) = 1$, gives

$$\Phi(\xi) = 1 + \int_0^\xi e^{-\int_0^\xi (n+3)F d\xi} \int_0^\xi 4n F' \Phi e^{\int_0^\xi (n+3)F d\xi} d\xi - \int_0^\xi (n+3)F d\xi + \Phi'(0) \int_0^\xi e^{\int_0^\xi (n+3)F d\xi} d\xi \quad (D4)$$

Applying the boundary condition, $\Phi(\infty) = 0$, results in

$$\Phi'(0) = \frac{-\left(1 + \int_0^\infty e^{-\int_0^\xi (n+3)F d\xi} \int_0^\infty 4n F \Phi e^{\int_0^\xi (n+3)F d\xi} d\xi\right)}{\int_0^\infty e^{-\int_0^\xi (n+3)F d\xi} d\xi} \quad (D5)$$

which is the temperature gradient at the fin surface.

The procedure begins by assuming an approximate temperature profile, $\Phi(\xi)$, for the case $n = 0$. Since from (D1), $F''' = -\Phi$, the corresponding function $F''(\xi)$ may be found by numerically integrating $\Phi(\xi)$ and using the appropriate boundary conditions to give

$$F''(\xi) = \int_\xi^\infty \Phi(\xi) d\xi. \quad (D6)$$

The functions $F'(\xi)$ and $F(\xi)$ are obtained in the same manner by integrating $F''(\xi)$ and $F'(\xi)$ respectively.

Thus,

$$\begin{aligned} F'(\xi) &= \int_0^\xi F''(\xi) d\xi \\ F(\xi) &= \int_0^\xi F'(\xi) d\xi. \end{aligned} \quad (D7)$$

Several of the integrals involved require integration from 0 to ∞ . It is obvious from figure 2.2 that integration

from $\xi = 0$ to 3 is sufficient for these integrals. All integrals are evaluated using the trapezoidal rule and increments of 0.05.

Once all the functions and integrating factors have been evaluated $\Phi'(0)$ may be determined from (D5) and then the new temperature distribution, $\Phi(\xi)$, evaluated from (D4). It is now necessary to check this new distribution with the original assumed $\Phi(\xi)$ for each numerical value of ξ , which goes from 0 to 3 in increments of 0.05. Obviously if the assumed distribution were correct there would be no difference between the two profiles. However if for any value of ξ considered, the two distributions vary by more than the set limit of 0.001, the new values of $\Phi(\xi)$ are now used as the starting profile and the procedure is repeated. This type of iteration is carried out until the difference between starting and final profiles, $\Phi(\xi)$, for every value of ξ considered, is less than 0.001.

When used, this procedure gave temperature and velocity profiles, for values of n up to 0.4, almost identical to those presented in the thesis. For larger values of n difficulty was encountered with the exponential, $\text{EXP} \int_0^\xi (n+3) F d\xi$, since the exponent became larger than that allowed in the computer. However it is quite possible the exponential may be split into parts and this problem overcome. This procedure, though not complete, is included here because of its potential as a method for solving problems of this type.


```

$IBFTC ALTSOL NOLIST,NODECK
  DIMENSION F(200),F3(3,200),SUM(200),F2(200),F1(200),F0(200),Q(200)
  1,QQ(200),QR(200),QS(200),QT(200),QU(200),QV(200),Q1(200)
  DIMENSION U(200),UA(500)
  M=10
  N=80
  TT=N
  EE=0.05
  F(1)=1.000000
  DO 1 J=2,N
  P=J
  X=(P-1.)/20.
  Y=X**1.4
  1 F(J)=.9530*EXP(-Y)
  DO 30 K=1,M
  R=K
  H=(R-1.)/10.
  WRITE(6,50)H
  LL=0
  G=1.0
  I=2
  I1=I-1
  DO 2 J=1,N
  2 F3(I,J)=F(J)
  20 DO 41 J=1,N
  41 F3(I1,J)=F3(I,J)
C     F3 IS EQUIVALENT TO TEMP, NOT NEG TEMP
  I=I-1
  SUMM=0.000000
  SUM(1)=0.000000
  DO 3 J=2,N
  J1=J-1
  SUM(J)=(F3(I,J1)+F3(I,J))*EE
  3 SUMM=SUMM+SUM(J)
  F2(1)=SUMM
C     F2(1) IS THE VELOCITY GRADIENT AT THE WALL
  DO 4 J=2,N
  SUMM=SUMM-SUM(J)
  4 F2(J)=SUMM
  SUMM=0.000000
  F1(1)=0.000000
  DO 5 J=2,N
  J1=J-1
  SUM(J)=(F2(J1)+F2(J))*EE
  SUMM=SUMM+SUM(J)
  5 F1(J)=SUMM
  SUMM=0.000000
  F0(1)=0.000000
  DO 6 J=2,N
  J1=J-1
  SUM(J)=(F1(J1)+F1(J))*EE
  SUMM=SUMM+SUM(J)
  6 F0(J)=SUMM
C     Q(J) IS THE INTEGRAL OF THE INTEGRATING FACTOR
  Q(1)=0.000000
  SUMM=0.000000
  DO 7 J=2,N
  J1=J-1
  SUM(J)=(H+3.)*(F0(J1)+F0(J))*EE
  SUMM=SUMM+SUM(J)

```



```

7      Q(J)=SUMM
     DO 18 J=1,N
18      Q1(J)=Q(J)/10.
C      QQ(J) IS VEL*TEMP*INTEGRATING FACTOR
19      DO 8 J=1,N
8      QQ(J)=F3(I,J)*F1(J)*((EXP(Q1(J)))*10)
C      QR(J) IS THE INTEGRAL OF QQ(J)
     QR(1)=0.000000
     SUMM=0.000000
     DO 9 J=2,N
     J1=J-1
     SUM(J)=(QQ(J1)+QQ(J))*FE
     SUMM=SUMM+SUM(J)
9      QR(J)=SUMM
C      QS(J) IS QR(J)* INVERSE OF INTEGRATING FACTOR
     QS(1)=0.000000
     DO 10 J=2,N
10     QS(J)=QR(J)*((EXP(-Q1(J)))*10)
C      QT(J) IS THE DOUBLE INTEGRAL
     QT(1)=0.000000
     SUMM=0.000000
     DO 11 J=2,N
     J1=J-1
     SUM(J)=4.*H*(QS(J1)+QS(J))*EE
     SUMM=SUMM+SUM(J)
11     QT(J)=SUMM
     DO 12 J=1,N
12     QU(J)=((EXP(-Q1(J)))*10)
     SUMM=0.000000
     QV(1)=0.000000
     DO 13 J=2,N
     J1=J-1
     SUM(J)=(QU(J1)+QU(J))*EE
     SUMM=SUMM+SUM(J)
13     QV(J)=SUMM
C      QV(J) IS THE INTEGRAL OF THE INVERSE OF INT FACTOR
     C=-(1.000000+QT(N))/QV(N)
C      C IS THE TEMP GRADIENT AT THE WALL
     I=I+1
     I1=I-1
     DO 16 J=1,N
16     F3(I,J)=1.000000+ C*QV(J)+QT(J)
     IF(LL.GT.0) GO TO 40
     L=1
     SUMM=0.000000
     DO 21 J=1,N
     U(J)=0.01*(ABS(F3(I,J)-F3(I1,J)))
     SUMM=SUMM+U(J)
21     UA(L)=SUMM/TT
     DO 22 J=1,N
22     F3(I,J)=F3(I,J)+G*U(J)*F3(I,J)
     L=L+1
     LL=LL+1
     GO TO 20
40     SUMM=0.000000
     DO 31 J=1,N
     U(J)=0.01*(ABS(F3(I,J)-F3(I1,J)))
     SUMM=SUMM+U(J)
     UA(L)=SUMM/TT
     Z=ABS(UA(L))

```



```
W=ABS(UA(L-1))
IF(Z.GT.W)G=-G
IF(Z.LT.0.000001) GO TO 15
DO 23 J=1,N
23  F3(I,J)=F3(I,J)+G*U(J)*F3(I,J)
L=L+1
GO TO 20
15  CONTINUE
WRITE(6,51)C
DO 14 J=1,N
S=J
XI=(S-1.)/20.
14  WRITE(6,53) XI,F0(J),F1(J),F2(J),F3(I,J)
DO 30 J=1,N
30  F(J)=F3(I,J)
STOP
50  FORMAT(2X,23HTEMPERATURE EXPONENT = ,F8.4/)
51  FORMAT(2X,24HTEMP GRADIENT AT WALL = ,F14.8/)
53  FORMAT(2X,F8.4,4F20.8)
55  FORMAT(2X,8E16.8)
END
$ENTRY ALTSOL
```


B29863